STARS

Electronic Theses and Dissertations, 2004-2019

2016

Microgrid Control and Protection: Stability and Security

Morteza Keshavarztalebi
University of Central Florida

Showcase of Text, Archives, Research & Scholarship

MICROGRID CONTROL AND PROTECTION: STABILITY AND SECURITY

by

MORTEZA KESHAVARZTALEBI
M.Sc. in Electrical Engineering, North Carolina A and T State University, NC, 2010
B.Sc. in Electrical Engineering, University of Guilan, Iran, 2005

A dissertation submitted in partial fulfilment of the requirements
for the degree of Doctor of Philosophy
in the Department of Electrical Engineering and Computer Science
in the College of Engineering and Computer Science
at the University of Central Florida
Orlando, Florida

Summer Term
2016

Major Professor: Aman Behal

ABSTRACT

When the microgrid disconnects from the main grid in response to, say, upstream disturbance or voltage fluctuation and goes to islanding mode, both voltage and frequency at all locations in the microgrid have to be regulated to nominal values in a short amount of time before the operation of protective relays. Motivated by this, we studied the application of intelligent pinning of distributed cooperative secondary control of distributed generators in islanded microgrid operation in a power system. In the first part, the problem of single and multi-pinning of distributed cooperative secondary control of DGs in a microgrid is formulated. It is shown that the intelligent selection of a pinning set based on the number of its connections and distance of leader DG/DGs from the rest of the network, i.e., degree of connectivity, strengthens microgrid voltage and frequency regulation performance both in transient and steady state. The proposed control strategy and algorithm are validated by simulation in MATLAB/SIMULINK using different microgrid topologies. It is shown that it is much easier to stabilize the microgrid voltage and frequency in islanding mode operation by specifically placing the pinning node on the DGs with high degrees of connectivity than by randomly placing pinning nodes into the network. In all of these research study cases, DGs are only required to communicate with their neighboring units which facilitates the distributed control strategy.

Historically, the models for primary control are developed for power grids with centralized power generation, in which the transmission lines are assumed to be primarily inductive. However, for distributed power generation, this assumption does not hold since the network has significant resistive impedance as well. Hence, it is of utmost importance to generalize the droop equations, i.e., primary control, to arrive at a proper model for microgrid systems. Motivated by this, we proposed the secondary adaptive voltage and frequency control of distributed generators for low and medium voltage microgrid in autonomous mode to overcome the drawback of existing classi-

cal droop based control techniques. Our proposed secondary control strategy is adaptive with line parameters and can be applied to all types of microgrids to address the simultaneous impacts of active and reactive power on the microgrids voltage and frequency. Also, since the parameters in the network model are unknown or uncertain, the second part of our research studies adaptive distributed estimation/compensation. It is shown that this is an effective method to robustly regulate the microgrid variables to their desired values.

The security of power systems against malicious cyberphysical data attacks is the third topic of this dissertation. The adversary always attempts to manipulate the information structure of the power system and inject malicious data to deviate state variables while evading the existing detection techniques based on residual test. The solutions proposed in the literature are capable of immunizing the power system against false data injection but they might be too costly and physically not practical in the expansive distribution network. To this end, we define an algebraic condition for trustworthy power system to evade malicious data injection. The proposed protection scheme secures the power system by deterministically reconfiguring the information structure and corresponding residual test. More importantly, it does not require any physical effort in either microgrid or network level. The identification scheme of finding meters being attacked is proposed as well. Eventually, a well-known IEEE 30-bus system is adopted to demonstrate the effectiveness of the proposed schemes.

ACKNOWLEDGMENTS

First, I would like to express my deepest appreciation to my advisor Prof. Aman Behal for the continuous support of my Ph.D study, for his patience, motivation, and immense knowledge. His guidance helped me through my research and the writing of this dissertation. I could not have imagined having a better advisor and mentor for my Ph.D study.

I also need to express my sincere gratitude to Dr. Saeed Manaffam without whose guidance and persistent help this dissertation would not have been possible. I also need to express my sincere thanks to Dr. Amit Jain, whose support and advice was very helpful and important to me. I would also like to thank the other members of my committee for reviewing my dissertation, providing feedback and advice and attending my defense: Dr. Nasser Kutkut, Dr. Michael Haralambous and Dr. Wei Sun.

TABLE OF CONTENTS

LIST OF FIGURES

LIST OF TABLES

CHAPTER 1: INTRODUCTION

Power system is the backbone of a country's economy and it has evolved in the last two decades to meet the rapid changes in consumer demands, decrease CO_2 emission, governmental incentives, and using alternative energy resources. The US Energy Information Administration (EIA) estimates that by 2040 consumption of renewable energy will be about 25% of the total world energy consumption and U.S. holds second place in its investments on renewable energy sector after China [1].

During past decades, significant changes have been made to power systems, however, any meaningful impact of smart technologies on the power system operation yet to be seen. The need for this transformation from conventional bulk power system to an intelligent one brought new concepts which are called smart grid and microgrid [2–5]. Based on the U.S. Department of Energy, the microgrid is identified as "a group of interconnected loads and distributed energy resources (DERs) with clearly defined electrical boundaries that acts as a single controllable entity with respect to the grid and can connect and disconnect from the grid to enable it to operate in both grid-connected or islanded mode" [6] [7]. Thus, the proper control of microgrid is a requirement for stable and economically efficient operation in both grid connected and islanded mode. In addition to the control of output active and reactive power flow, voltage and frequency regulation of DERs are the main criteria of the microgrid control structure in both operating modes [8] [9] [10].

When the microgrid is connected to the main grid, voltage and frequency of DERs are dictated from the main grid but in the case of upstream disturbance or voltage fluctuation, the microgrid disconnects from the main grid and goes to islanding mode. In the islanding mode operation, the so-called primary control is insufficient to maintain the voltage and frequency stability of DERs. Therefore, the secondary control should be applied to restore the DERs' voltage and frequency to

the nominal values.

In the microgrid, the stability of voltage and frequency of DERs is achieved by the primary control which is implemented by droop characteristics technique, which emulates the behavior of synchronous generator [11–14]. The droop employs the fact that in power systems, the frequency depends mostly on the active power, while the voltage depends mostly on the reactive power. However, due to the linearity of the droop equations, the voltage and frequency of DG's cannot adjust automatically to nominal operation point of the network, hence the offset values in these equations should be calculated by some other means [8] [15]. One of the prominent approaches to set the offset values in droop equations is to introduce a secondary control [10] [16]. Conventional secondary controls have a centralized structure and requires communications between the central controller and all individual distributed generators (DG) [10] [17] [18]. In this technique, complex and expensive communication infrastructure may be required while the failure in the central controller or the communication links can obscure the functionality of the secondary control and consequently, the performance of the network. To alleviate these issues, the secondary control can be implemented in a distributed and cooperative manner where a sparse and reliable communication network can be employed. One of the main advantages of the distributed cooperative control is that it tolerates certain changes in the underlying topology of the microgrid and it is robust to communication link failures. Given the inherent dynamism in power systems, e.g., plug and play, this feature makes the cooperative approach a suitable candidate for regulating the microgrids.

Distributed cooperative control has been investigated and successfully applied in various fields [19] [20]. The application of cooperative control for distributed generator (DG) operation in power systems in grid connected mode was introduced in [21] where the dynamics of the inverter was neglected. The consensus control of microgrid based on distributed secondary frequency control with a strict assumption of lossless power network model was proposed in [22]. The work of [22] has been extended in [23] with the addition of secondary voltage control for a lossy power

network model. The application of the cooperative control in maintaining the microgrid voltage and frequency in the islanded mode of operation using energy storage system is investigated in [24].

To drive the network to its nominal operation point, the nominal values for voltage and frequency should be provided to cooperative controller in one or multiple DGs. This technique of providing the reference values in distributed systems is called *pinning* where a fraction of the systems in the network have the reference values [25]. Pinning based control for network synchronization based on simulation results has been studied in [26] [27]. In [28], pinning control in microgrid islanding mode using energy storage system (ESS) as master unit was recently studied. In [29], Bidram *et al* employed multi-agents distributed cooperative secondary voltage control of the microgrid. The objective of the paper was that each DG would operate and converge to the reference voltage value dictated by the leader/master distributed generator in autonomous operation mode of the microgrid.

In these studies, the selection of the leader DG(s) has been assumed to be arbitrary. However, as it has been shown in [30–32], the performance and robustness of the network is directly related to choice of the leader(s). Motivated by this gap, in this paper, first we formulate the problem of single and multi pinning of multi agent distributed cooperative control in microgids. The DG dynamics in our tracking synchronization problem is adopted from [29]. Next, the effect of proper selection of pinning DG('s) is analyzed. Then we propose a suboptimal algorithm based on degree and distance of the candidate leader(s) from the rest of the microgrid. We also show that intelligent selection of the pinning point(s) (Leader DG/DGs) would result in faster convergence and further robustness of DG's terminal profiles both in transient and steady state, ensuring the stability of the microgrid. Also flexibility and effectiveness of the proposed algorithm are presented in the simulation results for several power system topologies and communication networks in Chapter 3.

The intelligent pinning of DGs in microgrid autonomous mode has been geared towards microgrid and DGs with fixed and known system parameters, i.e. control gain and weight of the communi-

cation links are assumed constant and ideal. In practice, it is desirable to have an adaptive control model that compensates for the nonlinear and uncertain dynamics of DGs and communication network. The adaptive voltage and frequency gain controller scheme is proposed in Chapter 4. The proposed controller applied together with conventional DG droop equation and secondary intelligent cooperative controller to real time, calculate the voltage and frequency gain controller and communication links gain controller to minimizes system transients in the islanding process and to ensure microgrid stability. The proposed control technique and numerical results have been shown in Chapter 4.

Additionally this research considered the generalized droop equation in which both R and X parameters of the line are reflected to address the simultaneous impacts of active and reactive power fluctuations on the microgrids voltage and frequency. Based on that we formulate the problem of adaptive distributed cooperative control in the microgrids to overcome the drawback of conventional droop based control methods and improve the power sharing and voltage regulation. Our proposed secondary control strategy is adaptive with line parameters and can be applied to all types of microgrids. Flexibility and effectiveness of the proposed control technique are presented in the simulation results for microgrid with different line parameters and communication networks in Chapter 4.

Finally in this dissertation, an enhanced protection scheme against malicious false data injection is proposed in Chapter 5. An algebraic criterion is derived to ensure a trustworthy power system against malicious cyber-physical data attacks. The proposed protection scheme takes advantage of expansive nature of power grids, reconfigures its subsystem data structure deterministically, and makes it impossible to organize a successful injection. The identification scheme for finding meters being attacked is proposed as well. The effectiveness of proposed protection scheme has been shown in IEEE 30 bus system.

CHAPTER 2: INTELLIGENT PINNING COOPERATIVE SECONDARY CONTROL

System Model

Primary Control

The frequency and voltage of each DG is controlled by regulation of the active and reactive powers, respectively. This is called droop controller

$$
\begin{cases}
\omega_{n_i} - \omega_i = m_{P_i} P_i, \\
V_{n_i} - V^\star_{i,mag} = n_{Q_i} Q_i,
\end{cases}
\tag{2.1}
$$

where ω_i and $V^\star_{i,mag}$ are the frequency and voltage amplitude of the ith DG, respectively; P_i and Q_i are the active and reactive powers going out of the ith DG. ω_{n_i} and V_{n_i} are reference angular frequency and voltage set point for droop equation, respectively; and m_{P_i} and n_{Q_i} are droop coefficients, respectively.

Inherent trade-off between the active and reactive power sharing and the frequency and voltage amplitude accuracy in droop controller, results in the frequency and voltage deviation from the nominal set points. Thus, it is desirable to deploy additional controller to restore the frequency and amplitude deviations produced by the primary droop controllers. A centralized secondary control is designed to set the references V_n and ω_n in (2.1) to restore nominal values of microgrid and to compensate for voltage-frequency deviations. However, limits and restrictions in centralized

controller method such as complex and expensive communication infrastructure, black out of the whole microgrid in case of failure of the central controller, and the need for redesigning the central controller in the case of installing/uninstalling new DGs, make it undesirable [33]. Hence to dynamically adjust the nominal values in primary controller, we will use distributed control method. However, prior to designing the cooperative controller, a model of DG is required.

Modeling of Inverter Based DG

The block diagram of voltage source inverter (VSI) based DG is shown in Fig. 2.1.
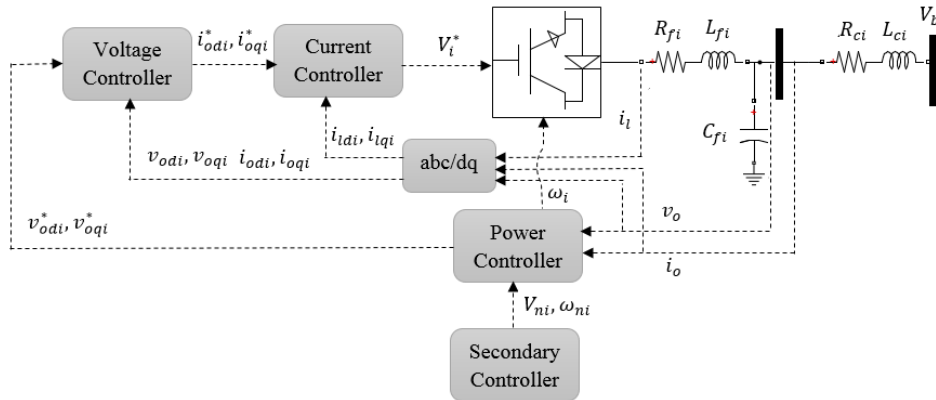
Figure 2.1: Inverter DG block diagram

This model consists of three legged inverter bridge connected to DC voltage source such as solar photovoltaic cells. The DC bus dynamics and switching process of the inverter can be neglected due to the assumption of ideal DC source from DG side and realization of high switching frequency of the bridge, respectively [29] [34].

The primary controller of a DG inverter consists of three parts: power, voltage, and current con-

trollers which set the voltage magnitude and frequency of the inverter [34] [35]. As shown in Fig. 4.4, the control process of primary controller are expressed in $d - q$ coordinate system. The objective of the primary controller is to align the output voltage of each DG on $d-$axis to the inverter 's reference frame and set the $q-$axis reference to zero

$$
\begin{cases}
V^\star_{od_i} = V_{n_i} - n_{Q_i} Q_i, \\
V^\star_{oq_i} = 0.
\end{cases}
\tag{2.2}
$$

The instantaneous active and reactive powers of inverter output are passed through low pass filters with cut-off frequency of ω_c to obtain the fundamental component of active and reactive powers: P_i and Q_i. The dynamics of the power controller can be written as [29] [34]

$$
\dot{P}_i = -\omega_{c_i} P_i + \omega_{c_i}(v_{od_i} i_{od_i} + v_{oq_i} i_{oq_i})
\tag{2.3a}
$$

$$
\dot{Q}_i = -\omega_{c_i} Q_i + \omega_{c_i}(v_{oq_i} i_{od_i} - v_{od_i} i_{oq_i}).
\tag{2.3b}
$$

The state and algebraic equations of voltage controller are

$$
\dot{\phi}_{d_i} = V^\star_{od_i} - V_{od_i},
\tag{2.4c}
$$

$$
\dot{\phi}_{q_i} = V^\star_{oq_i} - V_{oq_i},
\tag{2.4d}
$$

$$
i^\star_{ld_i} = F_i i_{od_i} - \omega_b C_{f_i} V_{oq_i} + K_{PVi}(V^\star_{od_i} - V_{od_i}) + K_{IVi}\phi_{di},
\tag{2.4e}
$$

$$
i^\star_{lq_i} = F_i i_{oq_i} + \omega_b C_{f_i} V_{od_i} + K_{PVi}(V^\star_{oq_i} - V_{oq_i}) + K_{IV_i}\phi_{qi},
\tag{2.4f}
$$

and the state and algebraic equations of current controller are as follows

$$\dot{\gamma}_{d_i} = i^{\star}_{ld_i} - i_{ld_i}, \tag{2.5g}$$

$$\dot{\gamma}_{q_i} = i^{\star}_{lq_i} - i_{lq_i}, \tag{2.5h}$$

$$V^{\star}_{id_i} = -\omega_b L_{f_i} i_{lq_i} + K_{PC_i}(i^{\star}_{ld_i} - i_{ld_i}) + K_{IC_i}\gamma_{d_i}, \tag{2.5i}$$

$$V^{\star}_{iq_i} = \omega_b L_{f_i} i_{ld_i} + K_{PC_i}(i^{\star}_{lq_i} - i_{lq_i}) + K_{IC_i}\gamma_{q_i}, \tag{2.5j}$$

where the $(V^{\star}_{od_i}, V^{\star}_{oq_i})$ are the voltage references for inner voltage controller loop provided by power controller, $(\dot{\phi}_{d_i}, \dot{\phi}_{q_i})$ and $(\dot{\gamma}_{d_i}, \dot{\gamma}_{q_i})$ are the auxiliary state variables defined for PI controllers for voltage and current control loop, respectively; K_{pvi}, K_{VI_i}, K_{PC_i}, K_{IC_i} are the parameters of the PI controller of the DG i, ω_b is the nominal angular frequency, F_i is current feed forward gain, $[L_{f_i}, C_{f_i}]$ are the elements of LC filter, $(i^{\star}_{ld_i}, i^{\star}_{lq_i})$ are the reference values for inner current controller loop of the DG provided by voltage controller. A complete state-space small-signal model and dynamics of the the ith inverter can be found in [29] [34].

Distributed Cooperative Control

A secondary voltage and frequency control of DGs in islanding operation is introduced in [29] [36]. The proposed controller is based on distributed cooperative controller design for a output feedback linearized model of the plant.

Secondary Voltage Control

The objective of secondary voltage controller is to synchronize the voltages of the terminals of all DGs to reference value dictated by leader DG via the communication matrix.

The procedure of designing the secondary voltage control by neglecting the fast dynamic respond of the primary control is

$$V_{od_i} = V_{n_i} - n_{Q_i}Q_i, \tag{2.6k}$$

$$V_{oq_i} = 0. \tag{2.6l}$$

By differentiating (2.6k), the droop dynamics can be expressed as

$$\dot{V}_{od_i} = \dot{V}_{n_i} - n_{Q_i}\dot{Q}_i \equiv u_{v_i}, \tag{2.7}$$

where u_{v_i} is an auxiliary control input to substitute the actual control input V_{n_i} for primary control in (2.1). Hence, the secondary voltage control of microgrid can be expressed as

$$\begin{cases} \dot{V}_{od_1} = u_{v_1} \\ \dot{V}_{od_2} = u_{v_2} \\ \vdots \\ \dot{V}_{od_N} = u_{v_N} \end{cases} \tag{2.8}$$

In addition, (2.8) represents the input-output feedback linearization of the microgrid. To synchronize the voltage of the ith DG to the nominal value via the communication network, the u_{v_i} is chosen as

$$u_{v_i} = -c_v e_{v_i}, \tag{2.9}$$

where c_v is the control gain and e_{v_i} is the local tracking error of the ith DG with respect to the reference signal and the neighboring DG's

$$e_{v_i} = \sum_{j=1}^{N} a_{ij}(V_{od_i} - V_{od_j}) + g_i\zeta_i(V_{od_i} - V_{ref}), \tag{2.10}$$

9

where $\mathbf{A} = [a_{ij}]$ is the adjacency matrix of the communication network, $a_{ij} = 1$ indicates a connection from j^{th} DG to i^{th} DG and otherwise $a_{ij} = 0$; g_i is the pinning gain of the ith DG and $\zeta_i \in \{0, 1\}$ indicates which nodes are pinned to the reference value. Hence, the primary control input, V_{n_i}, can be calculated as

$$V_{n_i} = \int (u_{v_i} + n_{Q_i}\dot{Q}_i)dt, \tag{2.11}$$

where the dynamics of Q_i is given in (2.3a).

Secondary frequency control

The objective of the secondary frequency controller is to synchronize the angular frequency of all the DGs to reference the value dictated by the leader DG via the communication matrix. The system dynamics for calculating the reference angular frequency of ω_n for primary controller can be obtained by differentiating the frequency droop characteristics as

$$\dot{\omega}_i = \dot{\omega}_{n_i} - m_{P_i}\dot{P}_i \equiv u_{\omega_i}, \tag{2.12}$$

where u_{ω_i} is an auxiliary control input to substitute the actual control input ω_{n_i} for primary control in (2.1). Hence, the secondary frequency control of microgrid for the networked DGs can be expressed as

$$\begin{cases} \dot{\omega}_1 = u_{\omega_1} \\ \dot{\omega}_2 = u_{\omega_2} \\ \vdots \\ \dot{\omega}_N = u_{\omega_N} \end{cases}. \tag{2.13}$$

10

To ensure the frequency synchronization of the ith DG to the reference value, the u_{ω_i} is chosen as

$$u_{\omega_i} = -c_\omega e_{\omega_i}, \tag{2.14}$$

where c_ω is the control gain and e_{ω_i} is the local tracking error of the ith DG with respect to the reference signal and the neighboring DGs

$$e_{\omega_i} = \sum_{j=1}^{N} a_{ij}(\omega_i - \omega_j) + g_i \zeta_i (\omega_i - \omega_{ref}), \tag{2.15}$$

where $\mathbf{A} = [a_{ij}]$ is the adjacency matrix of the communication network, $a_{ij} = 1$ indicates a connection from j^{th} DG to i^{th} DG and otherwise $a_{ij} = 0$; g_i is the pinning gain of the ith DG and $\zeta_i \in \{0, 1\}$ indicates which nodes are pinned to the reference value.

In the microgrid with N DG's, load demand is shared among the DG units proportional to the active power rating of units. Hence, the slopes ω-P should satisfy

$$m_{P_1} P_1 = \cdots = m_{P_i} P_i. \tag{2.16}$$

Therefore, by defining additional distributed cooperative frequency control for $m_{P_i} \dot{P}_i$ for the ith DG in (2.12) as u_{P_i} to satisfy (2.16) as

$$u_{p_i} = -c_p e_{p_i}, \tag{2.17}$$

where c_p is the control gain and e_{pi} is the local tracking error of the ith DG with respect to the neighboring DGs

$$e_{p_i} = \sum_{j=1}^{N} a_{ij}(m_{P_i} P_i - m_{P_j} P_j). \tag{2.18}$$

Therefore, according to (2.12)-(2.18), the primary control input, ω_n, can be calculated as

$$\omega_{n_i} = \int (u_{\omega_i} + u_{p_i})dt. \tag{2.19}$$

Control Problem Definition

Differentiating from (2.10) and substituting from (2.8), we have

$$\dot{e}_{v_i} = \sum_{i=1}^{N} a_{ij}(u_{v_i} - u_{v_j}) + g_i\zeta_i u_{v_i}, \tag{2.20}$$

which can be rewritten as

$$\dot{\mathbf{e}}_v = (\mathbf{L} + \mathbf{G}\,\mathbf{Z})\mathbf{u}_v, \tag{2.21}$$

where $\mathbf{e}_v = [e_{v_1}, e_{v_2}, \cdots, e_{v_N}]^T$ is the output voltage tracking error of the network,

$\mathbf{u}_v = [u_{v_i}, \cdots, u_{v_N}]^T$ is the auxiliary control input of the network, $\mathbf{G} = \mathrm{diag}([g_1, g_2, \cdots, g_N])$ is the network's pinning gain matrix, $\mathbf{Z} = \mathrm{diag}([\zeta_1, \zeta_2, \cdots, \zeta_N])$ is the pinning matrix, and $\mathbf{L} = [l_{ij}]$ is the Laplacian matrix of the communication network defined as

$$l_{ij} = \begin{cases} -a_{ij} & i \neq j \\ \sum_{j=1}^{N} a_{ij} & i = j. \end{cases} \tag{2.22}$$

Substituting $\mathbf{u}_v$ from (2.9) in (2.20), the tracking error dynamics for voltage can be derived as

$$\dot{\mathbf{e}}_v = -c_v(\mathbf{L} + \mathbf{G}\,\mathbf{Z})\mathbf{e}_v. \tag{2.23}$$

Similar to voltage synchronization formulation, the dynamics of angular frequency error can be

obtained by differentiating from (2.15) and substituting $\mathbf{u}_\omega$ from (2.14)

$$\dot{\mathbf{e}}_\omega = -c_\omega(\mathbf{L} + \mathbf{G}\,\mathbf{Z})\mathbf{e}_\omega. \tag{2.24}$$

As it is known from linear time-invariant system theory, the performance and robustness of the systems in (2.23) and (2.24) are directly dependent on the eigenvalues of $\mathbf{L} + \mathbf{G}\,\mathbf{Z}$. For instance, the convergence rate of the distributed errors for voltage and frequency are $c_v\lambda_{\min}(\mathbf{L} + \mathbf{G}\,\mathbf{Z})$ and $c_\omega\lambda_{\min}(\mathbf{L} + \mathbf{G}\,\mathbf{Z})$, respectively. Therefore, choosing which DG(s) to provide the reference values, i.e., $\mathbf{Z}$, carries an important role on performance of the microgrid. This problem can be formulated as

Problem 1. *Let* $\mathbf{G} = g\mathbf{I}_N$ *and the number of desired pinning nodes be* m_0*, then*

$$\begin{aligned} \mathbf{Z}^\star &= argmax \ \phi(\mathbf{Z}, g) \\ s.\ t. \quad &\|\mathbf{Z}\|_0 = m \\ &\mathbf{Z} = diag([\zeta_1 \cdots \zeta_N]), \ \zeta_i \in \{0,\ 1\} \ \forall i \in \mathcal{N}, \end{aligned} \tag{2.25}$$

where $\|\cdot\|_0$ *denotes norm* 0*, and* $\phi(\mathbf{Z}) \triangleq \lambda_{\min}(\mathbf{L} + g\mathbf{Z})$*.*

Another problem of interest is to minimize the number of pinning nodes while guaranteeing a certain convergence rate, $\lambda^\star$, which can be formulated as

Problem 2. *Let* $\lambda^\star$ *be the desired convergence rate and* $\mathbf{G} = g\mathbf{I}_N$*, then*

$$\begin{aligned} \min \quad &\|\mathbf{Z}\|_0 \\ s.\ t. \quad &\phi(\mathbf{Z}, g) \geq \lambda^\star \\ &\mathbf{Z} = diag([\zeta_1 \cdots \zeta_N]), \ \zeta_i \in \{0,\ 1\} \ \forall i \in \mathcal{N}, \end{aligned} \tag{2.26}$$

where $\phi(\mathbf{Z}) \triangleq \lambda_{\min}(\mathbf{L} + g\mathbf{Z})$*.*

As it has been shown, the optimal solution of problem in (2.25) and (2.26) are NP-hard, i.e., their solutions have exponential complexity. Due to exponential complexity of the optimal solution in microgrids with large number of DGs, finding the optimal solution is not practical which renders the suboptimal solutions with polynomial time complexity to be of immense interest [30–32, 37]. This is the topic which we will pursue in the next section.

Main Results

The following will be used in the sequel. Let assume that the nodes $\mathcal{I}_0 = \{i_1, \cdots, i_{m_0}\}$ are pinned, this is called the pinning set. Let the farthest node to pinning set, $\mathcal{I}_0$, be k. Then define the set $\mathcal{I}_j, \forall j \in \{1, \cdots, k\}$ as

$$\mathcal{I}_j = \left\{ i \,\middle|\, a_{pi} = 1, \forall p \in \mathcal{I}_{j-1}, \, i \in \mathcal{N} \setminus \bigcup_{m=1}^{j-1} \mathcal{I}_m \right\}, \qquad (2.27)$$

where a_{pi} are entries of the adjacency matrix of the communication network, $\mathcal{N} = \{1, \cdots, N\}$, and $\setminus$ denotes minus operation for sets.

Fig. 2.2 illustrates the sets defined in (2.27).

For each set in (2.27), we define the following

$$d_{i,j}^{\text{out}} = \sum_{p \in \mathcal{I}_{j+1}} a_{pi}, \quad i \in \mathcal{I}_j, \qquad (2.28)$$

$$d_{i,j}^{\text{in}} = \sum_{p \in \mathcal{I}_{j-1}} a_{ip}, \quad i \in \mathcal{I}_j, \qquad (2.29)$$

where $\mathcal{I}_{-1} = \mathcal{I}_{k+1} = \emptyset$. Please note, due to the definition in (2.27), $d_{i,j}^{\text{out}} \geq 1, \forall j \in \{0, \cdots, k-1\}$.

In the first step to solve Problem 1, let the number of pinning nodes, $\mathcal{I}_0 = \{i\}$. This is called single pinning method.

Theorem 1. *[37, Theorem 2] Let the network be connected and undirected, and d_i denote the degree of the node i, then if $\mathcal{I}_0 = \{i\}$, we have*

$$\phi_l(\mathbf{L}, i, g) \leq \phi(\mathbf{L}, i, g) \leq \phi_u(\mathbf{L}, i, g), \tag{2.30}$$

where

$$\phi_u(\mathbf{L}, i, g) \triangleq \frac{g}{2} + \frac{Nd_i}{2(N-1)}$$
$$- \sqrt{\frac{g^2}{4} + \left(\frac{Nd_i}{2(N-1)}\right)^2 + \frac{(N-2)gd_i}{2(N-1)}}.$$

N is the network size, g is the pinning gain; The lower bound, $\phi_l(\mathbf{L}, i, g)$ is smallest positive root of the polynomials, $\alpha_i(\mu)$ $i = 0, \cdots, k-1$

$$\alpha_i(\mu) = d_{\min, i-1}^{out} + d_{i, \min}^{in} - \mu - d_{\max, i}^{in}{}^2 / \alpha_{i+1}(\mu), \tag{2.31}$$

where

$$\alpha_k(\mu) = d_{\min, k}^{in} - \mu$$

$$d_{\min, i}^{in} = \min_{j \in \mathcal{I}_i}(d_{j,i}^{in})$$

$$d_{\min, i}^{out} = \min_{j \in \mathcal{I}_i}(d_{j,i}^{out}))$$

$$d_{\max, i}^{in} = \max_{j \in \mathcal{I}_i}(d_{j,i}^{in})$$

$$d_{\min, -1}^{out} = g.$$

Remark 1. *$\phi_u(\mathbf{L}, i, g)$ have the following properties [37]*

- *$\phi_u(\mathbf{L}, i, g)$ is a strictly increasing function of pinning degree, d_i, and pinning gain g;*

- *$\phi_u(\mathbf{L}, i, g)$, is alway bounded by 1,*

$$\phi_u(\mathbf{L}, i, g) \leq \lim_{g \to \infty} \phi_u(\mathbf{L}, i, g) \leq \frac{d_{\max}}{N - 1},$$

  where $d_{\max}$ is the maximum degree in the network. This implies that no matter how large the pinning gain is chosen, in single pinning strategy, the convergence rate of the errors in (2.23) and (2.24) cannot exceed c_v and c_ω, respectively;

- *In case the coupling network is a tree, Theorem 1 implies that the worst pinning nodes would be the end nodes and the most proper node to pin the network is the node with highest degree.*

Generalization of Theorem 1 to the case of multiple pinning can be given as

Theorem 2. *[37, Theorem 3] Let the communication network, $\mathbf{L}$, be connected and undirected.*

Given the pinning set, $\mathcal{I}_0$, with $m = |\mathcal{I}_0|$, then

$$\phi_l(\mathbf{L}, \mathbf{Z}, g) \leq \phi(\mathbf{L}, \mathbf{Z}, g) \leq \phi_u(\mathbf{L}, \mathbf{Z}, g), \tag{2.32}$$

where

$$\phi_u(\mathbf{L}, \mathbf{Z}, g) = \beta \left(1 - \sqrt{1 - \frac{\sum_{i=1}^{m} d_{0,i}^{in}{}^2}{(N-m)\beta^2}} \right) \tag{2.33}$$

$$\beta = \frac{\sum_{i=1}^{m} d_{i,0}^{out} + (N-m)(g + d_{\min,0}^{in})}{2(N-m)}.$$

The lower bound, $\phi_l(\mathbf{L}, \mathbf{Z}, g)$, is the smallest positive root of the polynomials, $\alpha_i(\mu)$ $i = 0, \cdots, k-1$

$$\alpha_i(\mu) = d_{\min, i-1}^{out} + d_{i, \min}^{in} - \mu - d_{\max, i}^{in}{}^2 / \alpha_{i+1}(\mu), \tag{2.34}$$

where

$$\alpha_k(\mu) = d_{\min, k}^{in} - \mu,$$

$$d_{\min, i}^{in} = \min_{j \in \mathcal{I}_i}(d_{j,i}{}^{in})$$

$$d_{\min, i}^{out} = \min_{j \in \mathcal{I}_i}(d_{j,i}{}^{out}))$$

$$d_{\max, i}^{in} = \max_{j \in \mathcal{I}_i}(d_{j,i}{}^{in})$$

$$d_{\min, -1}^{out} = g.$$

Remark 2. *$\phi_u(\mathbf{L}, \mathbf{Z}, g)$ have the following properties [37]*

- *$\phi_u(\mathbf{L}, \mathbf{Z}, g)$ is a strictly increasing function of pinning gain g;*

- $\phi_u(\mathbf{L}, \mathbf{Z}, g)$ *is always bounded by the size of pinning set,* m,

$$\phi_u(\mathbf{L}, \mathbf{Z}, g) \leq \lim_{g \to \infty} \phi_u(\mathbf{L}, \mathbf{Z}, g) \leq \frac{m d_{\max}}{N - 1}.$$

This implies that no matter how large the pinning gain is chosen, the convergence rate of the errors in (2.23) and (2.24) cannot exceed $m\, c_v$ *and* $m\, c_\omega$, *respectively;*

- *Also Theorem 2 indicates that the smaller the distance of the pinning set from the farthest node in the network, the higher is the lower bound, which in turn leads to better pinning performance. This will be illustrated in the numerical results.*

Algorithm

Based on remarks 1 and 2, in the previous section, the following heuristic algorithm can be given to solve Problem 2. This algorithm has linear search complexity and its pinning performance is very close to the optimal solution which has an exponential complexity.

Let us define

$$\mathcal{N} = \{1, \cdots, N\},$$
$$\mathcal{I} = \left\{ i \,\middle|\, d_i \geq \lfloor \mu^\star \rfloor + 1 \right\},$$
$$\mathcal{I}_0 = \mathcal{N} \setminus \mathcal{I} \quad : \text{set of nodes to be pinned,}$$

where

$$
\text{path}(i,\, \mathcal{I}_0) =
\begin{cases}
\text{shortest path length from} & \mathcal{I}_0 \neq \emptyset \\
\text{node i to super node} & \\
d_i & \mathcal{I}_0 =, \emptyset
\end{cases}
$$

$$
p_j(i,\, \mathcal{I}_0) = \text{number of path lengths of 1 from node } i
$$

$$
\text{to super node } \mathcal{I}_0,
$$

where $\mu^\star$ is the desired connectivity of the network to the reference node.

1. $\mathcal{I} = \{\, i \mid d_i \geq \lfloor \mu^\star \rfloor + 1 \,\}$

2. $\mathcal{I}_0 = \mathcal{N} \setminus \mathcal{I}$, and set $m_p = |\mathcal{I}_0|$

3. if $|\mathcal{I}_0| < m$ then

   (a) while $m_p \leq m$, do

   - $\text{path}(d_{i_1},\, \mathcal{I}_0) \geq \text{path}(d_{i_2},\, \mathcal{I}_0) \geq \cdots \geq \text{path}(d_{i_{|\mathcal{I}|}},\, \mathcal{I}_0)\ \forall i_j \in \mathcal{I}$,
   - if $\text{path}(d_{i_1},\, \mathcal{I}_0) = \cdots = \text{path}(d_{i_k},\, \mathcal{I}_0)$ then sort these nodes by $d_{i_j} - p_1(i_j, \mathcal{I}_0)$,
   - $\mathcal{I}_0 = \mathcal{I}_0 \cup \{i_1\}, \mathcal{I} = \mathcal{I} \setminus \{i_1\}$, and $m_p = |\mathcal{I}_0|$,

   (b) if $\mathbf{L} + g\mathbf{Z} - \mu^\star \mathbf{I}_N \succeq \mathbf{0}$, then stop

   else: set $m = m + 1$ and go to 3a.

4. if $|\mathcal{I}_0| = m$ then

   (a) if $\mathbf{L} + g\mathbf{Z} - \mu^\star \mathbf{I}_N \succeq \mathbf{0}$, then stop

   else: set $m = m + 1$ and go to 3a.

5. if $|\mathcal{I}_0| > m$ then

19

(a) while $m_p > m$ do

- path$(d_{i_1}, \mathcal{I}_0 \setminus \{i_1\}) \leq$ path$(d_{i_2}, \mathcal{I}_0 \setminus \{i_2\}) \leq \cdots \leq$ path$(d_{i_{|\mathcal{I}_0|}}, \mathcal{I}_0 \setminus \{i_{|\mathcal{I}_0|}\})$, $\forall i_j \in \mathcal{I}_0$,

- if path$(d_{i_1}, \mathcal{I}_0) = \cdots =$ path$(d_{i_k}, \mathcal{I}_0)$ then sort these nodes by $p_1(i_j, \mathcal{I}_0 \setminus \{i_j\}) - d_{i_j}$,

- $\mathcal{I}_0 = \mathcal{I}_0 \setminus \{i_1\}, \mathcal{I} = \mathcal{I} \cup \{i_1\}$, and $m_p = |\mathcal{I}_0|$,

(b) if $\mathbf{L} + g\mathbf{Z} - \mu^\star \mathbf{I}_N \succeq \mathbf{0}$, then stop

else: set $m = m + 1$ and go to 3a.

Since in Problem 1, there is no target $\mu^\star$, the algorithm starts with $\mu^\star = 0$ and m is set to the desired number of pinnings in the constraint; when the algorithm reaches the condition $\mathbf{L} + g\mathbf{Z} - \mu^\star \mathbf{I}_N \succeq \mathbf{0}$ in step 3-b, which is always satisfied, the algorithm stops with the size of pinning set $|\mathcal{I}_0| = m$.

This algorithm can also be used for a directed network. However, in a directed network, instead of using $\mathbf{A}$ in the calculations, $\mathbf{A}_{\text{new}} = \mathbf{A} + \mathbf{A}^T$, should be used.

Communication Topology in Microgrid

Due to the microgrid physical structure, any communication network topology and redundancy scheme can be readily configured depending on the requirement and cost targets [38]. The proposed intelligent pinning control must be supported by a local communication network that provides its required information flows. Our study cases uses both two ways and one-way communication links in the microgrid. [29] implemented its fully distributed control strategy through a communication network with one-way communication links. In the one-way communication link, we restrict the transition function so that the new state of the sender (pinning location) does not depend on the state of receiver (neighboring DG). It can be assumed that an interaction does not change the state of pinning DG/DGs at all. Also one-way communication link can be supported by plug and play operation capability of DGs and existence of communication hardware. Importance of location of DG and load in network topology i.e. if the DG is feeding any critical load or not can be considered as a cost effective decision factor to have one-way communication link as well. Communication between DGs in microgrid with small geographical span can be done through CAN Bus and PROFIBUS communication protocols [39]. It should be noted that although time delays are inherent in microgrid communication infrastructures but due to large time scale of secondary control, its effect on the microgrid performance is neglected. The secondary controllers are expected to operate five to ten times slower or more than the primary controllers [40].
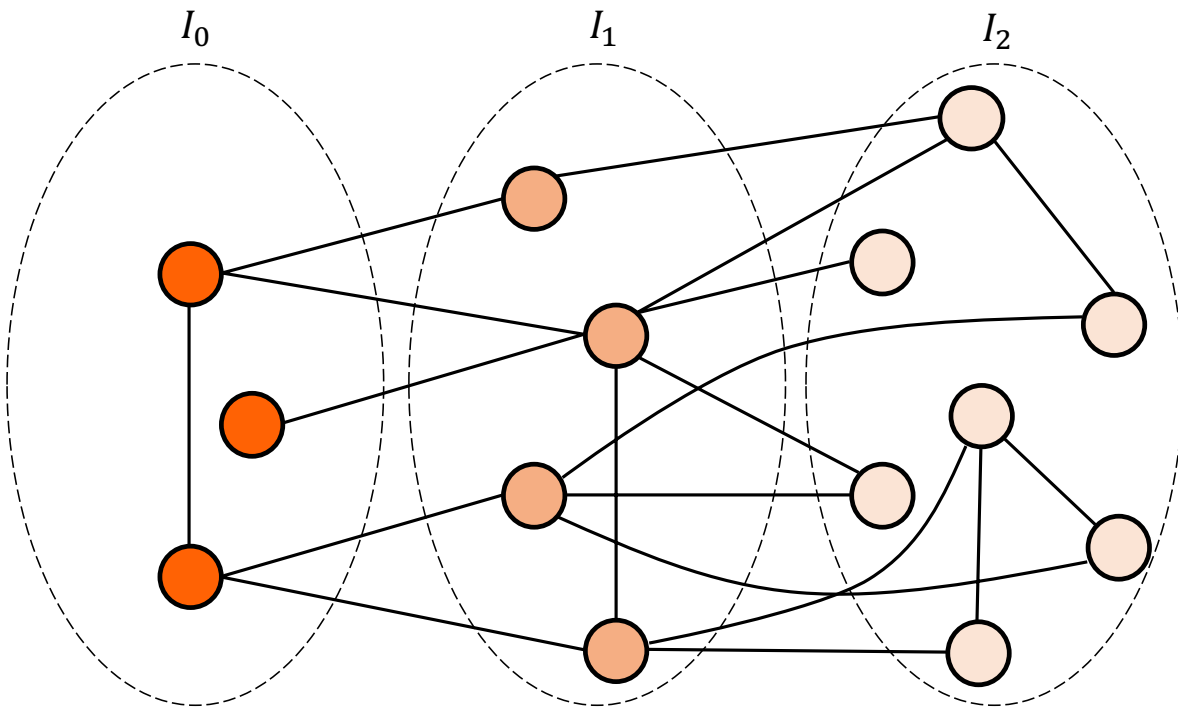
Figure 2.2: Sample topology where the farthest node from the pinning set, $\mathcal{I}_0$, is $k = 2$. $\mathcal{I}_0$ is assumed to be the pinning set.

CHAPTER 3: NUMERICAL RESULTS OF INTELLIGENT PINNING COOPERATIVE SECONDARY CONTROL

Main Results

In this section, we have used the Simpower System Toolbox of Simulink for 4 bus and 5 bus power systems with different topologies and communication networks to show the adaptability and effectiveness of the proposed control method. Microgrid operates on a 3-phase, 380V(L-L), and frequency of 50 Hz ($\omega_0 = 314.15(rad/s)$). DGs are connected through distribution series RL branches and loads are constant. In the first case study, single and multi pinning algorithm under directed and undirected communication networks is studied. The second case study investigates the application of single and multi pinning algorithm in undirected and failed link communication networks. And the final case study is a comparison of our single pinning algorithm with existing work. Optimal pinning gain value can be calculated based on communication network topology to adjust the speed of pinning control methodology. This study, in all cases, assumes the pinning gain is calculated offline and is set to $g = 1$. As mentioned earlier, an ideal DC source is assumed from DG side; therefore, the weather effect is not considered in this study. It should also be noted that the undershoot and overshoot of voltage amplitude and frequency of the DGs in microgrid during the transient from grid connected to islanding mode should not exceed 10-20 cycles to avoid the operation of 27, 59, and 81 protective relays. The protective power relay's voltage and frequency elements are typically set to $0.88\ (p.u.) \leq v_{\text{mag}} \leq 1.1\ (p.u.)$ and $47\ (Hz) \leq f \leq 50.5\ (Hz)$ for 10-20 cycles. The reminder of the network parameters, the specifications of DGs, and loads are given in the appendix.

Fig. 3.1 shows microgrid one-line diagram with the five bus ring system and its communication network.
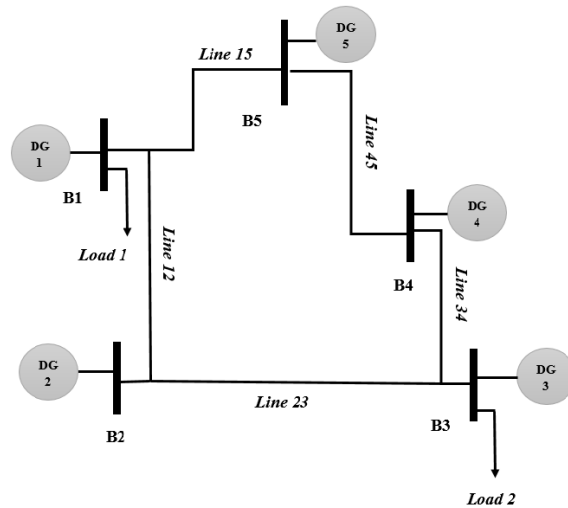
(a)
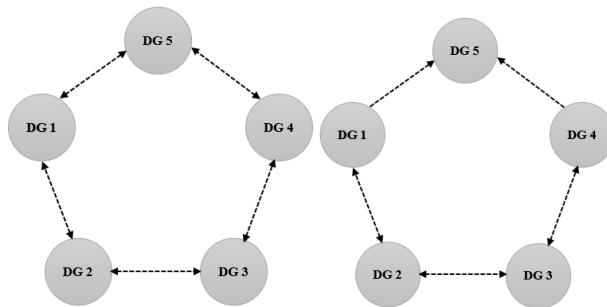
(b)   (c)

Figure 3.1: (*a*) Single line diagram of 5 bus ring system configuration network(dash arrows represent information flow):, (*b*) undirected communication network, (*c*) directed communication network.

Here, we consider the single and multi pinning methods for undirected and directed networks. In the undirected network case which is shown in Fig. 3.1b, all DGs are able to send and receive data from their immediate neighbors. In the directed network shown in Fig. 3.1c, DG1 and DG4 are not receiving any data from DG5. The microgrid's main breaker opens at $t = 0$ (s) and goes to the islanding mode at the same time the secondary voltage and frequency control are activated. DGs terminal voltage amplitudes and frequencies with the single pinning method are shown in Fig. 3.3 and Fig. 3.2 for two different communication networks corresponding to Fig. 3.1b and Fig. 3.1c, respectively.

In the undirected communication network of Fig. 3.1b, all DGs are able to send and receive data from their neighbors and all DGs are also equally located apart from each other, hence based on our proposed algorithm, the performance of the single pinning of any arbitrary DG is expected to be the same. It can be observed from Fig. 3.3 that the consensus is reached for the voltage and frequency and the steady state errors, $\frac{\|\mathbf{e}_{ssv}\|}{v_0}(\%), \frac{\|\mathbf{e}_{ssf}\|}{f_0}(\%)$, are zero. Application of intelligent pinning control for micrgrid voltage stabilization in lossless power system can be found at [37]. From Fig. 3.3 and Table 3.1, it can be seen that the performance of pinning any DGs are the same. For instance, when pinning DG3, the DGs terminal voltages and frequencies reach to the steady state values at $t_{s_v} = 0.26$ (s) and $t_{s_f} = 0.19$ (s) which are given in Fig. 3.3c, respectively. Pinning DG1 results in $t_{s_v} = 0.26$ (s) and $t_{s_f} = 0.19$ (s) as indicated in Fig. 3.3a.

Table 3.1: Single pinning of undirected 5 bus ring network given in Fig. 3.1b.

Pinning DG	t_{s_v}	t_{s_f}	$\frac{\|\mathbf{e}_{ss_v}\|}{V_{ref}}(\%)$	$\frac{\|\mathbf{e}_{ss_f}\|}{f_0}(\%)$
DG1	0.26 (s)	0.19 (s)	0.00%	0.00%
DG2	0.26 (s)	0.20 (s)	0.00%	0.00%
DG3	0.26 (s)	0.19 (s)	0.00%	0.00%
DG4	0.26 (s)	0.19 (s)	0.00%	0.00%
DG5	0.26 (s)	0.20 (s)	0.00%	0.00%

Table 3.1 gives the performance of the network given in Fig. 3.1b for several cases of single pinning in terms of settling time and the norm of all DGs terminal voltage and frequency errors from reference values. t_{s_v} and t_{s_f} denote the settling times for voltage and frequency, respectively. $\|\mathbf{e}_{ss_v}\|$ and $\|\mathbf{e}_{ss_f}\|$ denote the norm of network errors from the reference values for voltage and frequency, respectively. The error vectors for voltage and frequency are defined in (2.23) and (2.24), respectively. In the directed communication network given in Fig. 3.1c, for single pinning, $m = 1$ is set in Algorithm 1 and we have path$(DG1, \mathcal{N} \backslash \{DG1\}) = $ path$(DG4, \mathcal{N} \backslash \{DG4\}) = 7$, path$(DG2, \mathcal{N} \backslash \{DG3\}) = 6$ and path$(DG5, \mathcal{N} \backslash \{DG5\}) = \infty$. Since out degree of both DG2 and DG3 are the same, the algorithm predicts that the performance of the pinning, for pinning either one of the DGs, should be identical. As it can be seen from Figs. 3.2c and 3.2b, pinning DG2 and DG3 gives the same performance results, *i.e.*, $t_{s_v} = 0.24$ (s) and $t_{s_f} = 0.19$ (s). As determined by the algorithm and shown by the results in Fig. 3.2e, pinning DG5 will not help microgrid stabilization because it does not share any information with its neighboring DGs. As it can be seen from Figs. 3.2a and 3.2d, pinning DG1 and DG4 results in the microgird reaching its frequency stability at $t_{s_f} = 0.25$ (s) which exceeds the maximum allowance time setting point of frequency relay (20 cycle). Table 3.2 summarizes the performance of the network in Fig.3.1c for

several cases of single pinning in terms of settling time and the norm of all DGs terminal voltage and frequency errors from reference values. N/A in the row related to DG5 pinning location means microgrid did not stabilize at all. This is expected as DG5 does not share any information with the rest of the network.

Table 3.2: Single pinning of directed 5 bus ring network given in Fig. 3.1c.

Pinning DG	t_{s_v}	t_{s_f}	$\frac{\|\mathbf{e}_{ss_v}\|}{V_{ref}}(\%)$	$\frac{\|\mathbf{e}_{ss_f}\|}{f_0}(\%)$
DG1	0.34 (s)	0.25 (s)	0.00%	0.00%
DG2	0.24 (s)	0.19 (s)	0.00%	0.00%
DG3	0.24 (s)	0.19 (s)	0.00%	0.00%
DG4	0.34 (s)	0.25 (s)	0.00%	0.00%
DG5	N/A (s)	N/A (s)	N/A%	N/A%

Next, the effectiveness of the proposed multiple pinning method is studied. Fig.3.4 shows the evolution of the terminal voltages and frequencies when multiple DGs are pinned in the directed, *i.e.*, Fig. 3.1c, communication networks. The concept of pinning more than one DG can be used in the microgrid with a larger geographical span when the communication network would be more complex and costly [21]. It would also increases the robustness of the network to adverse events such as fault and/or communication failure among DGs. This advantage of multi-pinning method will be demonstrated in the next case study.

Figure 3.2: DGs terminal amplitudes voltage (at left) and frequency (at right) corresponding to Fig. 3.1c communication network: (a) Pinning DG1,(b) Pinning DG2, (c) Pinning DG3,(d) Pinning DG4, (e) Pinning DG5.

28
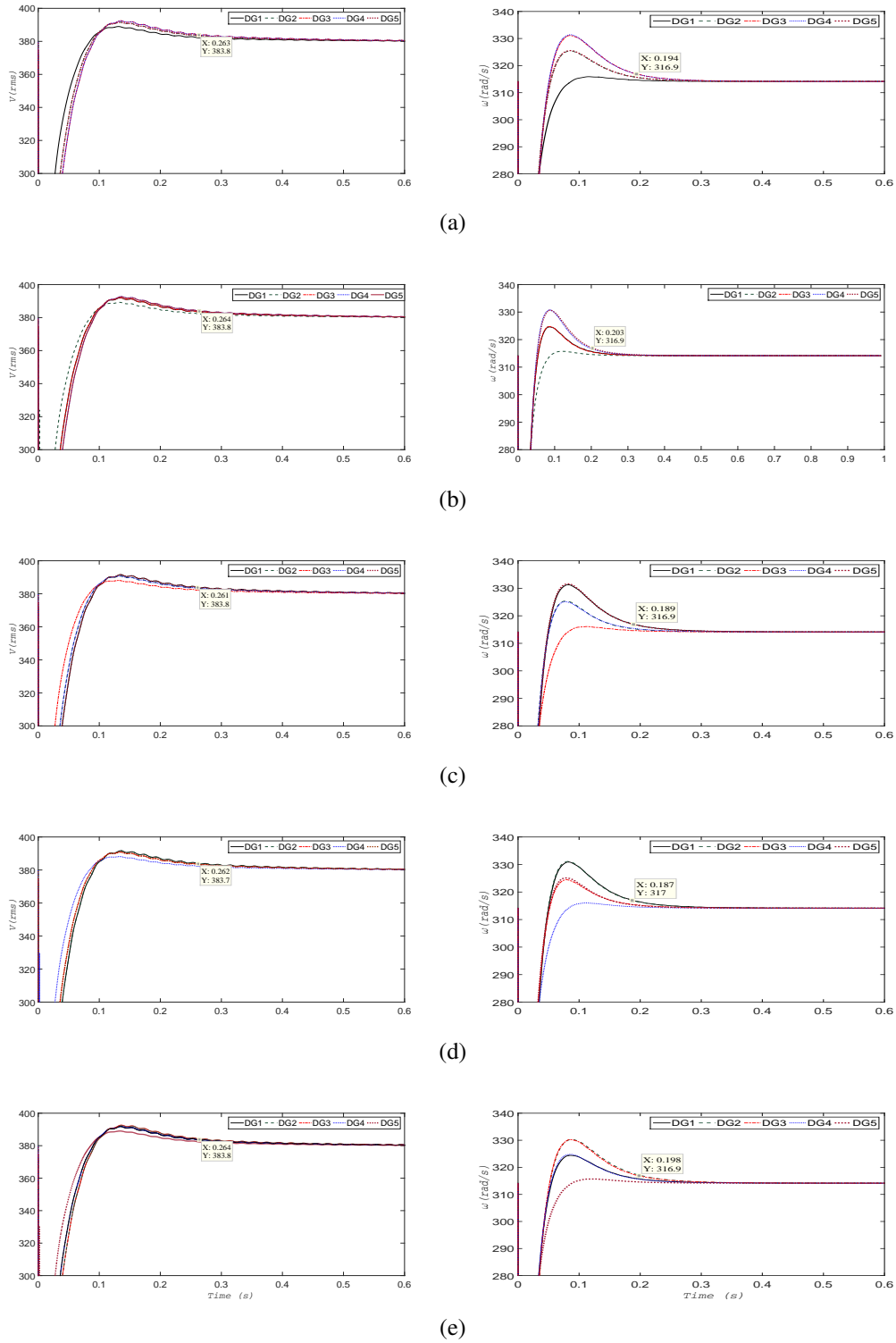
Figure 3.3: DGs terminal voltage amplitudes (at left) and frequency (at right) corresponding to Fig. 3.1b communication network: (a) Pinning DG1, (b) Pinning DG2, (c) Pinning DG3, (d) Pinning DG4, (e) Pinning DG5.

29

If the desired number of nodes to be pinned is set to $m = 2$ in the first iteration as before, either DG2 or DG3 should be selected. If DG2 is selected, at the start of the second iteration, we have $\mathcal{I} = \{\text{DG1, DG3, DG4, DG5}\}$ and path($\{\text{DG2, DG1}\}, \mathcal{I} \setminus \{\text{DG1}\}$) = path(DG2, DG3, $\mathcal{I} \setminus \{\text{DG3}\}$) = path($\{\text{DG2, DG5}\}, \mathcal{I} \setminus \{\text{DG5}\}$) = 4 and path($\{\text{DG2, DG4}\}, \mathcal{I} \setminus \{\text{DG4}\}$) = 3. Therefore, for $m = 2$ the pinning is $\mathcal{P} = \{\text{DG2, DG4}\}$. If in the first iteration DG3 is selected, then path($\{\text{DG2, DG4}\}, \mathcal{I} \setminus \{\text{DG4}\}$) = 3 and the pinning set $\mathcal{P} = \{\text{DG1, DG3}\}$, which also predicts that the performance of the pinning $\{\text{DG1, DG3}\}$ is the same as pinning $\{\text{DG2, DG4}\}$. This can also be deduced from the symmetry in the network. Fig. 3.4 shows the evolution of the terminal voltages and frequencies when multiple DGs are pinned in the directed, *i.e.*, Fig. 3.1c, communication network. As observed from the results of pinning set of DG1 and DG3 in Fig. 3.4d, both DGs' terminal voltage and frequency reach to the reference value at $t_{s_v} = 0.08$ (s) and $t_{s_f} = 0.10$ (s) while pinning set of DG2 and DG4 in Fig. 3.4a results in $t_{s_v} = 0.08$ (s) and $t_{s_f} = 0.12$ (s). Several candidates with their corresponding performances are given in Table 3.3. As it can be seen, the proposed method of pinning results in much better performance both in transient over voltage and frequency and settling time of voltage and frequency for the microgrid. Also, as predicted by our algorithm, it can be observed from the results in Fig. 3.4c, that choosing DG5 as one of the candidates for pinning location set of DG2 and DG5, results in microgrid stability with poor performance because DG5 does not share any information with its neighbor.

Pinning DG	t_{s_v}	t_{s_f}	$\frac{\|\mathbf{e}_{ss_v}\|}{V_{ref}}(\%)$	$\frac{\|\mathbf{e}_{ss_f}\|}{f_0}(\%)$
DG1 and DG3	0.08 (s)	0.10 (s)	0.00%	0.00%
DG2 and DG4	0.08 (s)	0.12 (s)	0.00%	0.00%
DG3 and DG4	0.21 (s)	0.21 (s)	0.00%	0.00%
DG2 and DG5	0.26 (s)	0.17 (s)	0.00%	0.00%

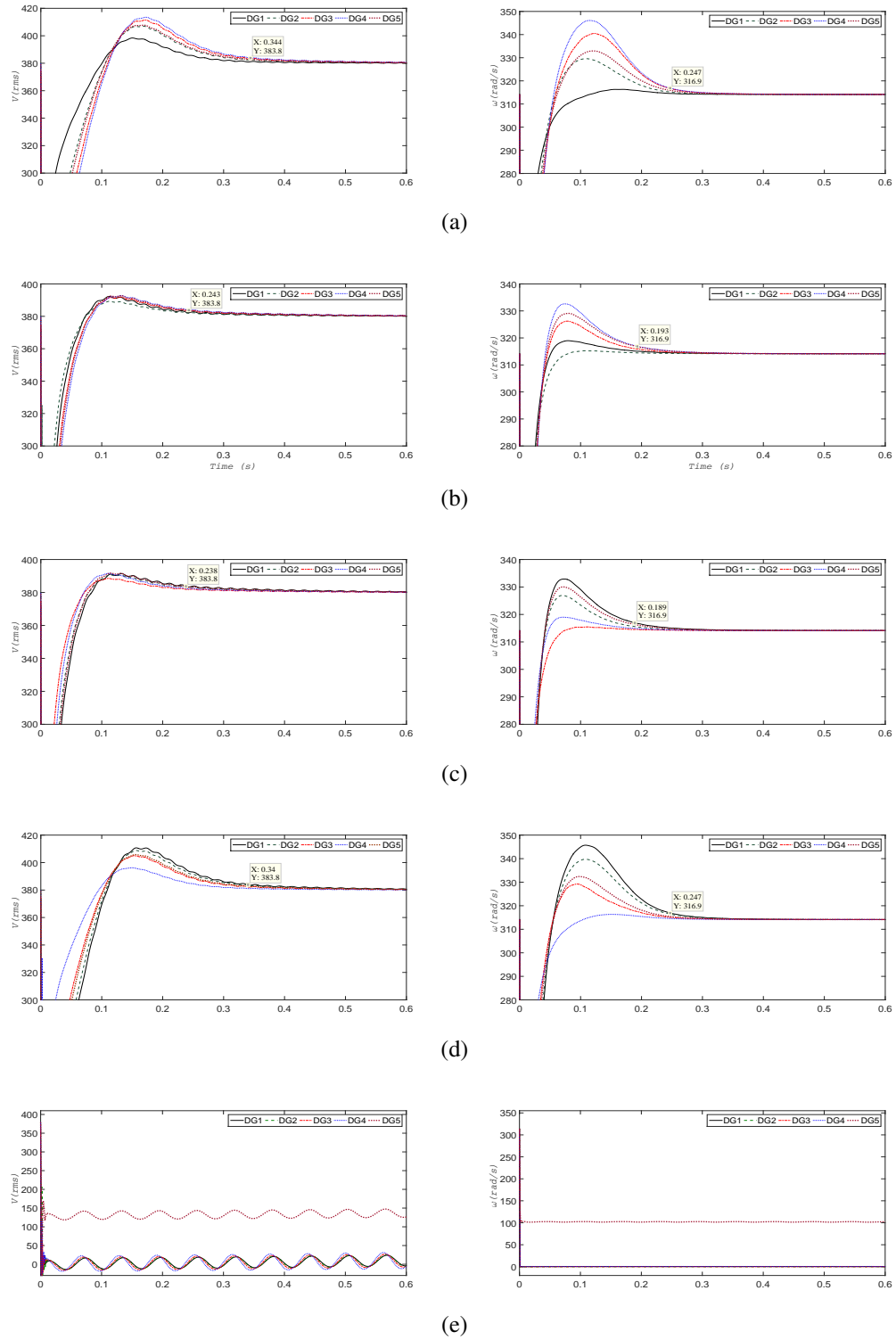Table 3.3: Multi pinning of 5 bus ring network given in Fig. 3.1c.
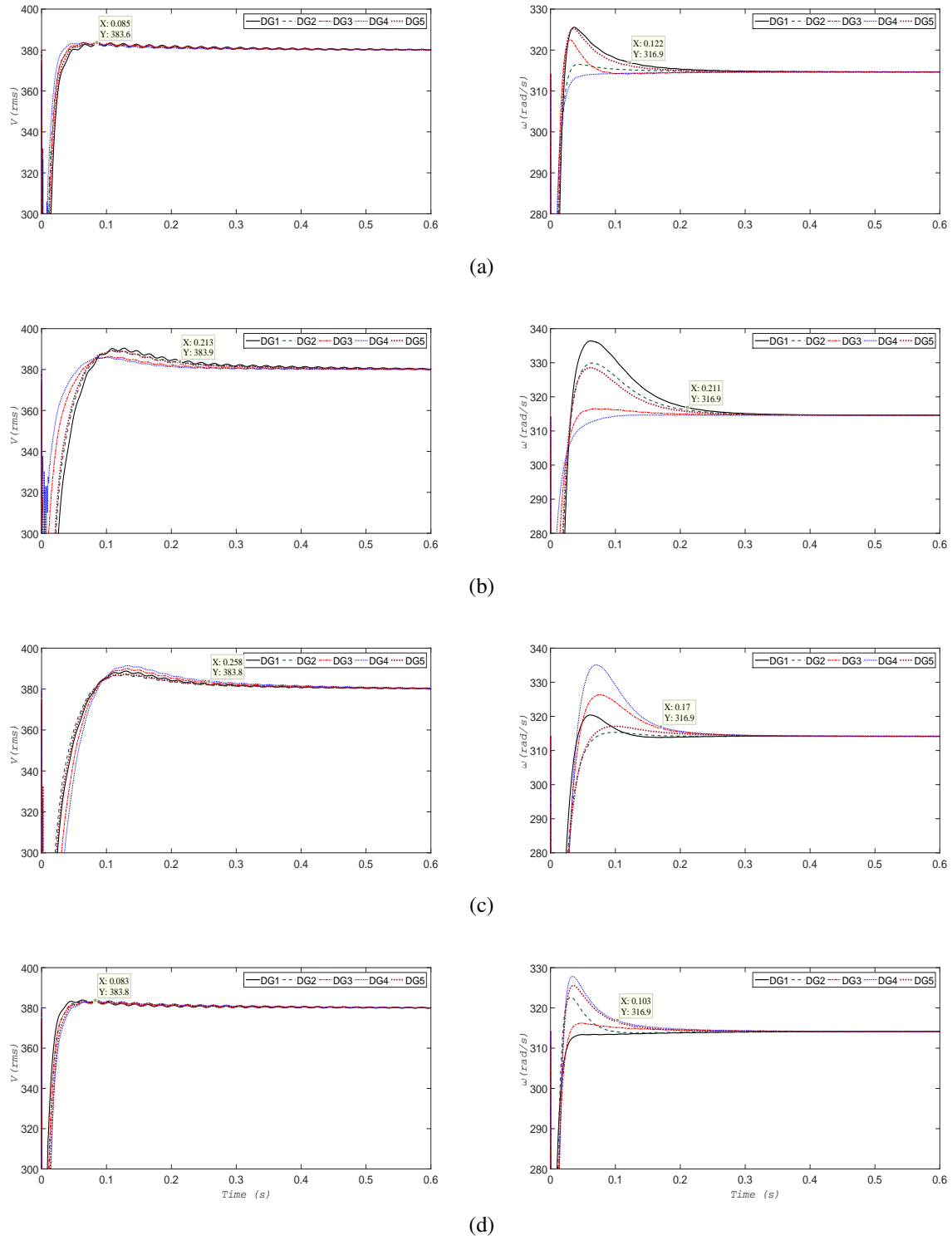
Figure 3.4: DGs terminal amplitudes voltage (at left) and frequency (at right) corresponding to Fig. 3.1c communication network: (a) pinning DG2 and DG4, (b) pinning DG3 and DG4, (c) pinning DG2 and DG5 (d) pinning DG1 and DG3.

31
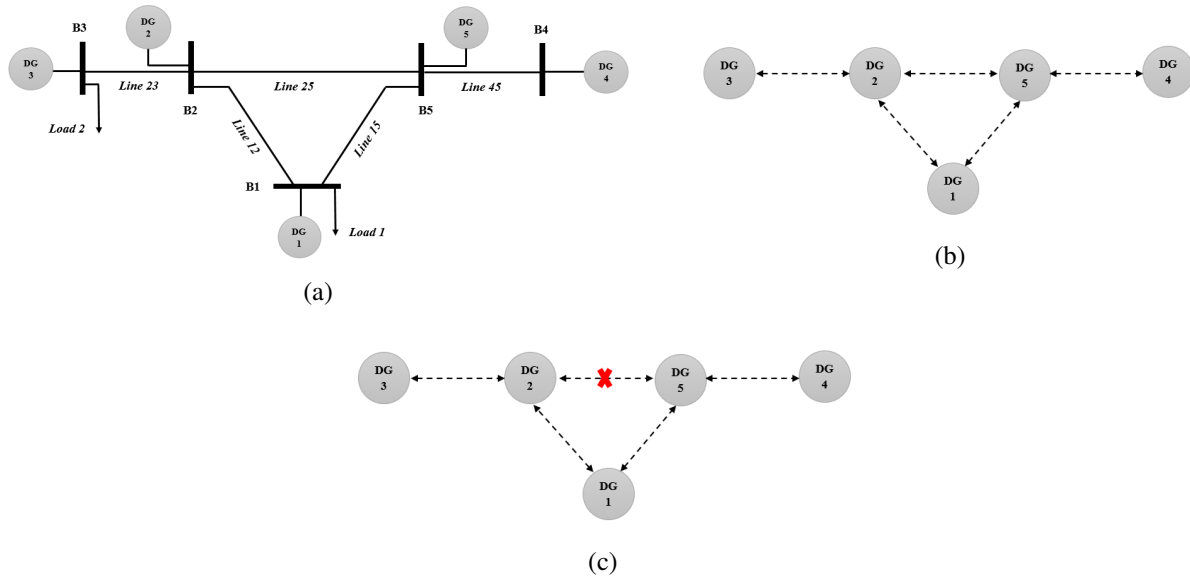
Figure 3.5: Single line diagram of 5 Bus system: (a) system configuration, (b) communication network, (c) communication network with failed link.

Case 2: Alternative Single and Multi-Pinning illustrative examples under undirected and failed link communication network

Another 5 bus topology with its communication network is shown in Fig. 3.5. In this example, two different communication networks are studied. First scenario follows the undirected communication topology, which is shown in Fig. 3.5b, and in the second scenario, it is assumed that there is a communication failure between DG2 and DG5 and that they cannot communicate with one another depicted in Fig 3.5c.

Similar to case study 1, the microgrid's main breaker opens at $t = 0$ (s) and goes to the islanding mode while secondary control is activated.

Multi-pinning of Fig. 3.5 with $m = 2$ is given in Fig. 3.6 and for the link failure in Fig. 3.7, following two communication network conditions as stated earlier: In the first scenario, the communication network is unchanged, Fig. 3.5b, while in the second scenario, the communication link between DG2 and DG5 failed, Fig. 3.5c. Following the proposed multi pinning scheme for Fig. 3.5b, our algorithm gives DG3 and DG5 , *i.e.*, $\mathcal{I}_0 = \{3, 5\}$ or DG2 and DG4, $\mathcal{I}_0 = \{2, 4\}$, as best pinning set location(s). These simulation results validate our proposed algorithm that choosing the pinning set of DG5/DG2 with a high degree of connectivity and communication links to their neighboring DGs and DG3/DG4, which is the furthest DG in respect to DG5/DG2, at the same time would help the voltage and frequency recovery of the microgrid in both transient response and steady state condition. Simulation results of DG2 and DG4 or DG3 and DG5 pinning sets are shown in Fig 3.6a and Fig. 3.6d, respectively, and validate our pinning algorithm strategy. As it was predictable, other arrangement sets of pinning nodes i.e. pinning DG1 and DG5 has poorer performance for network transient respond for microgrid islanding operation and its selling time is $t_{s_v} = 0.12$ (s) and $t_{s_f} = 0.19$ (s), shown in Fig 3.6b . Table 3.4 summarizes the results of different multi pinning sets for the microgrid related to Fig 3.5b. The simulation results also indicate the effectiveness of our proposed algorithm in the time of communication failure. Our algorithm chooses DG2 and DG5 for the best pinning location. It is important to recognize that the failed communication link between DG2 and DG5 can group the communication network of microgrid into two clusters of $(DG1, DG2, DG3)$ and $(DG1, DG5, DG4)$. Therefore, following our proposed algorithm in single pinning, selecting DG2 in the first cluster and DG5 in the second cluster as a pinning location with a high degree of connectivity will improve voltage and frequency of the microgrid both in transient response and steady state condition shown in Fig. 3.7d. Also, as determined by our multi pinning algorithm and the evidence indicated by the results in Figs. 3.7a and 3.7e, the performance of another pinning set arrangements, *i.e.*, DG3 and DG5 or DG2 and DG4 demonstrate the effectiveness of our proposed algorithm. Other pinning set arrangements such as DG1 and DG5 or DG1 and DG4 did not help the recovery of the islanded microgrid and may cause

the operation of under/over voltage protective relays before microgrid reaches to its stabilization. Table 3.5 reviews the several multi pinning set location results for micrgrid in Fig 3.5c.

Table 3.4: Multi pinning of alternative 5 bus network given in Figs. 3.5b.

Pinning DG	t_{s_v}	t_{s_f}	$\frac{\|\mathbf{e}_{ss_v}\|}{V_{ref}}(\%)$	$\frac{\|\mathbf{e}_{ss_f}\|}{f_0}(\%)$
DG2 and DG4	0.09 (s)	0.13 (s)	0.00%	0.00%
DG1 and DG5	0.12 (s)	0.19 (s)	0.00%	0.00%
DG1 and DG4	0.18 (s)	0.21 (s)	0.00%	0.00%
DG3 and DG5	0.07 (s)	0.15 (s)	0.00%	0.00%

Table 3.5: Multi pinning of alternative 5 bus network given in Figs. 3.5c.

| Pinning DG	t_{s_v}	t_{s_f}	$\frac{\|\mathbf{e}_{ss_v}\|}{V_{ref}}(\%)$	$\frac{\|\mathbf{e}_{ss_f}\|}{f_0}(\%)$
DG2 and DG4	0.09 (s)	0.09 (s)	0.00%	0.00%
DG1 and DG5	0.25 (s)	0.23 (s)	0.00%	0.00%
DG1 and DG4	0.27 (s)	0.27 (s)	0.00%	0.00%
DG2 and DG5	0.09 (s)	0.10 (s)	0.00%	0.00%
DG3 and DG5	0.06 (s)	0.10 (s)	0.00%	0.00%
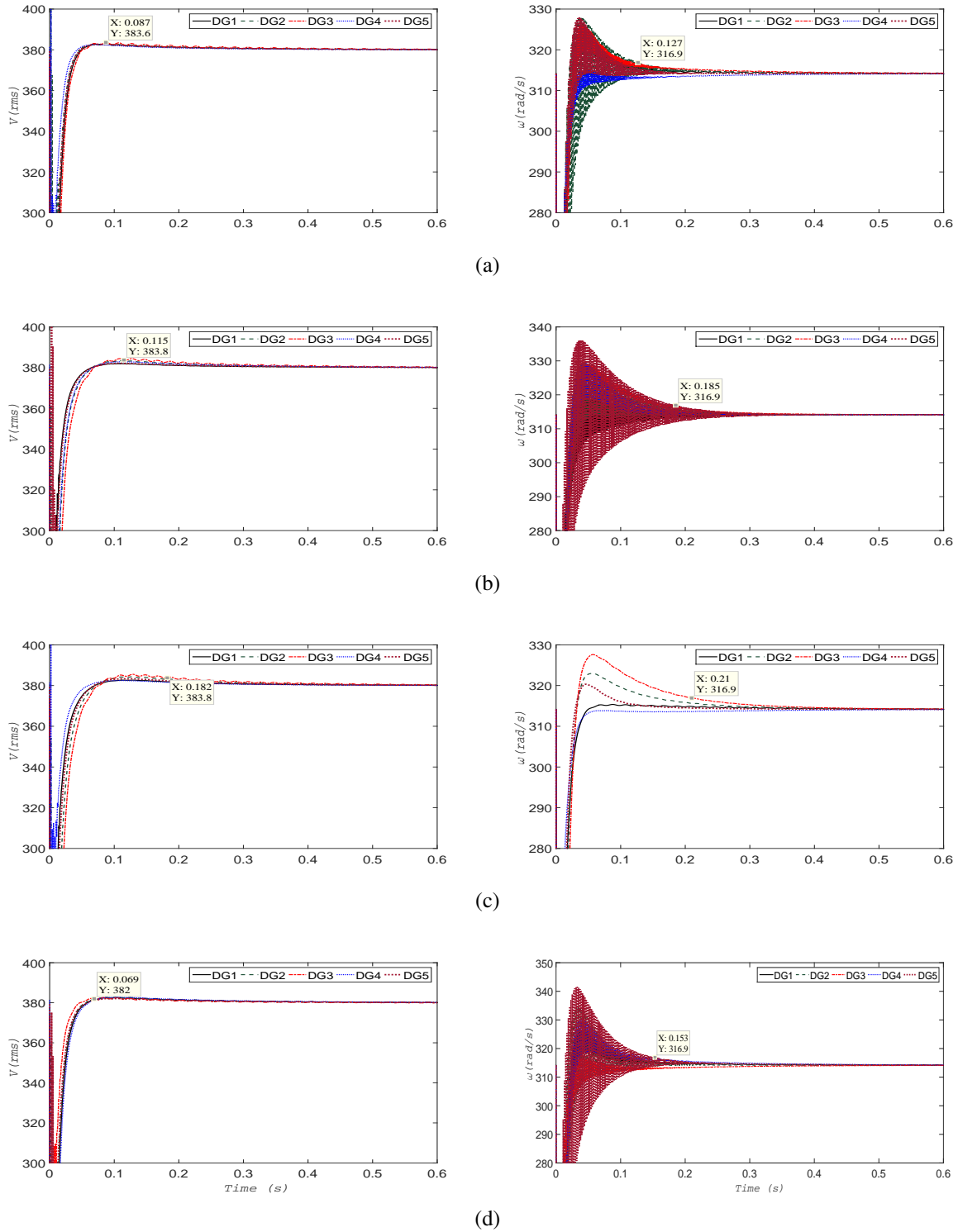
Figure 3.6: DGs terminal amplitudes voltage (at left) and frequency (at right) corresponding to Fig. 3.5b communication network: (a) pinning DG2 and DG4, (b) pinning DG1 and DG5, (c) pinning DG1 and DG4, (d) pinning DG3 and DG5.

35
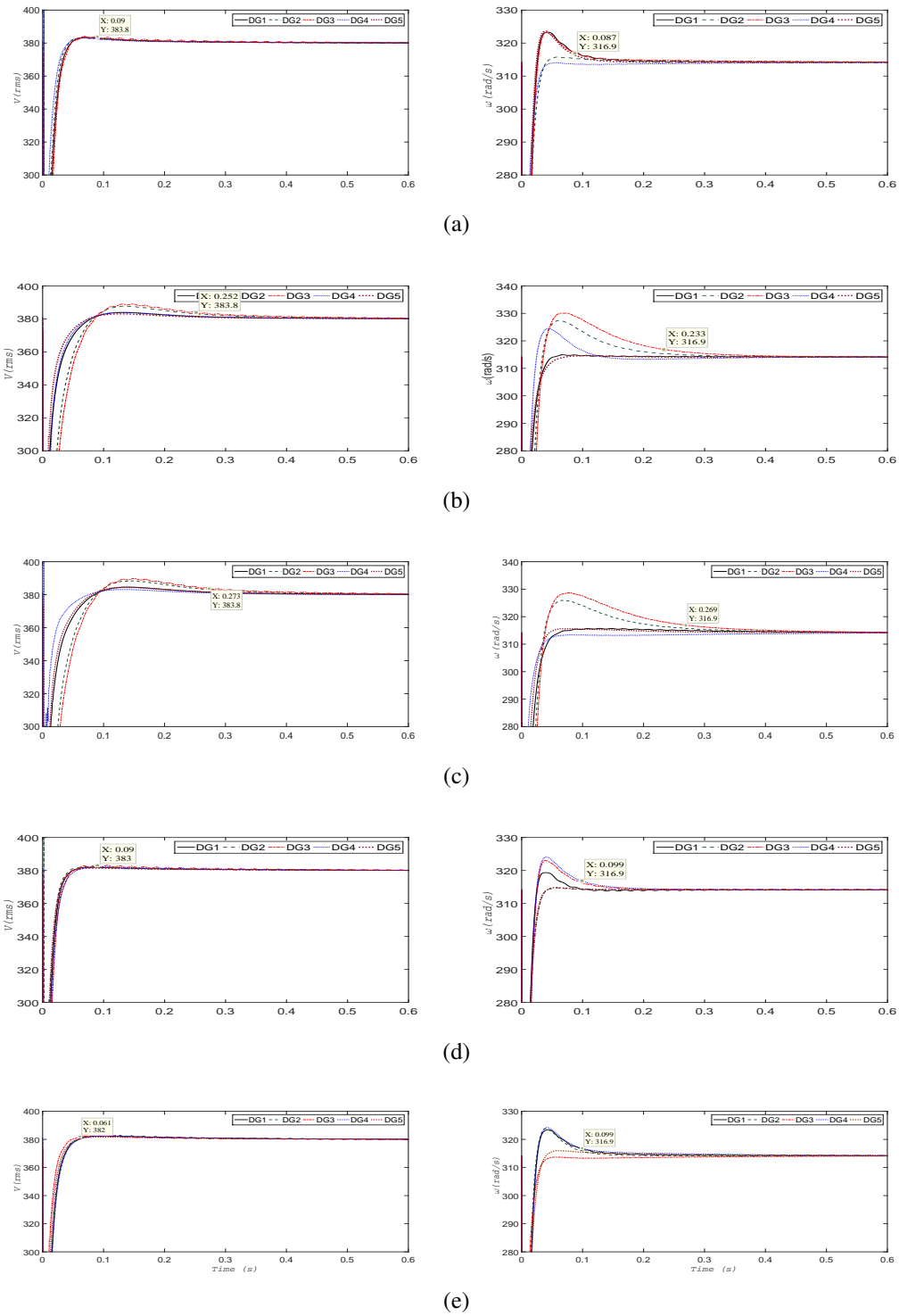
Figure 3.7: DGs terminal voltage amplitudes (at left) and frequency (at right) corresponding to Fig. 3.5c communication network: (*a*) pinning DG2 and DG4, (*b*) pinning DG1 and DG5, (*c*) pinning DG1 and DG4, (*d*) pinning DG2 and DG5,, (*e*) pinning DG3 and DG5.
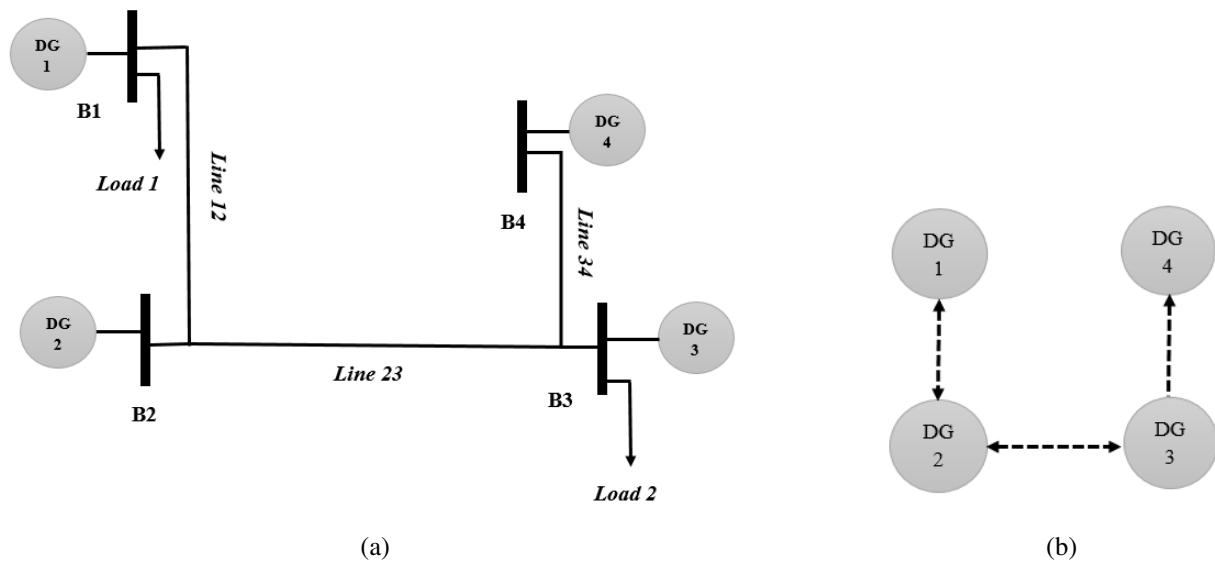
Figure 3.8: Single line diagram of 4 Bus system (dash arrows represent information flow): (a) system configuration, (b) communication network.

Case 3: Comparison with Existing Work

Here, we assume that the network is to be stabilized by single pinning method. The bus and communication networks are given in Fig. 3.8. In this configuration, it is assumed that the DGs communicate with each other through a fixed communication network shown in Fig. 3.8b.

The diagram shows that the DGs only communicate with their neighboring DG. In this scenario, the microgrid's main breaker opens at $t = 0$ (s) and it goes to the islanding mode while at the same time the secondary voltage and frequency control are initiated. DGs terminal voltage amplitude and frequency for different reference single pinning scenario are shown in Fig. 3.9. Based on the tracking synchronization control strategy, it can be seen that all DGs' terminal voltage and frequency return to the reference value dictated by the leader DG. However, pinning DG2 results in a faster and more robust convergence in comparison with DG1 presented in [29]. Please note

that in [29], because of its minimum directed communication topology, pinning DG1 is suggested while our pinning algorithm indicates that DG2 should be pinned, which also coincides with the optimal solution of Problem 1.

Table 3.6 provides information about settling time and the norm of all DGs' terminal voltage and frequency errors from reference value for both pinning cases. As it can be observed in Fig. 3.9c, pinning DG2 results in superior performance, *i.e.*, transient behavior as well as convergence rate, compared to pinning the other DGs in the network. It should be noted that DG4 cannot be selected as a leader because it does not share information with DG3 causing microgrid weaken performance similar to directed case study of pinning DG5 in Fig. 3.2e.

Table 3.6: Single pinning of 4 bus system given in 3.8.

Pinning DG	t_{s_v}	t_{s_f}	$\frac{\|\mathbf{e}_{ss_v}\|}{V_{ref}}(\%)$	$\frac{\|\mathbf{e}_{ss_f}\|}{f_0}(\%)$
DG1	0.26 (s)	0.23 (s)	0.00%	0.00%
DG2	0.16 (s)	0.13 (s)	0.00%	0.00%
DG3	0.28 (s)	0.18 (s)	0.00%	0.00%

We have introduced algorithms for stabilizing DGs' terminal voltage and frequency to their homogeneous state by intelligent pinning of microgrid nodes using their local communication network in distributed way, which deters the necessity of a centralized approach. The placement of the pinning node is affected by the topology of the network. It is shown that it is much easier to stabilize the microgrid voltage and frequency in islanding mode operation by specifically placing the pinning node on the DGs with high degrees of connectivity than by randomly placing pinning nodes into the network.
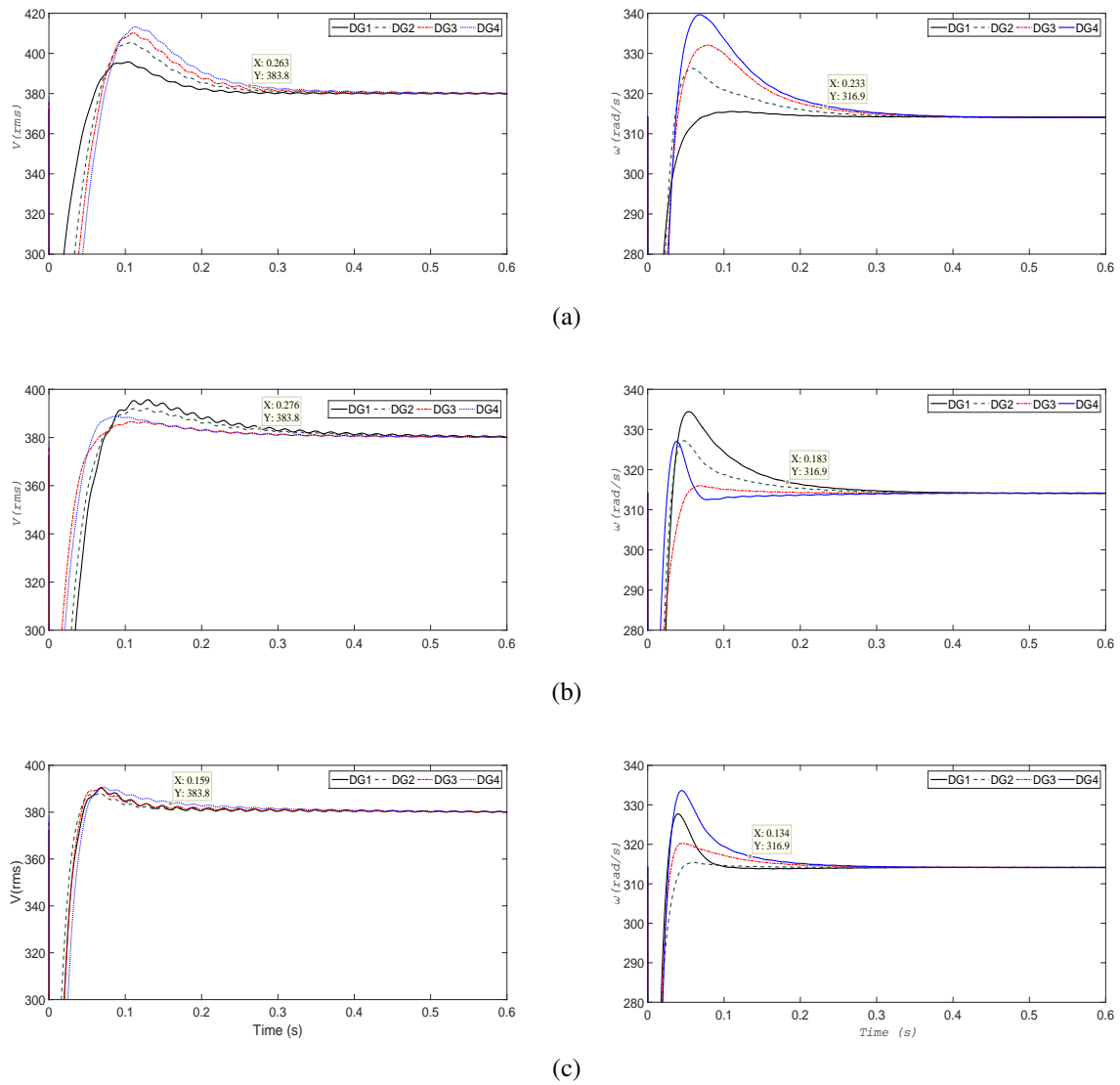
Figure 3.9: DGs terminal amplitudes voltages (at left) and frequency (at right) for several pinning scenarios corresponding to Fig. 3.8b (*a*) pinning DG1, (*b*) pinning DG2, (*c*) pinning DG3.

CHAPTER 4: ADAPTIVE SECONDARY CONTROL

Adaptive secondary voltage and frequency gain control

The stable operation of the microgrid capability to continue after disconnecting from the main grid depends directly upon its control strategy. As studied in previous chapters, the most common method to control the Distributed Generators (DGs) in microgrid is based on well-known conventional droop characteristics. A droop controller employs the fact that the microgrid voltage and frequency are dependent on active and reactive power, respectively. However, even in the presence of this primary control (Droop technique), DGs' voltage and frequency in autonomous operation can still diverge from it nominal values. Therefore, a further control level, distributed cooperative secondary control, is required to restore voltage and frequency values [29, 37].

In chapter 3, we proposed the intelligent pinning of DGs in microgrid autonomous mode. However, this has been geared towards microgrid and DGs with fixed and known system parameters, i.e. control gain and weight of the communication links are assumed constant and ideal. In practice, it is desirable to have an adaptive control model that compensates for the nonlinear and uncertain dynamics of DGs and communication network.

The proposed adaptive control scheme, applied together with DG droop controls and secondary intelligent cooperative voltage and frequency controller to real time, calculate the voltage and frequency gain controller in addition to weights of communication links in microgrid to minimizes system transients in the islanding process and to ensure microgrid voltage and frequency stability.

A secondary distributed cooperative voltage and frequency control of DGs in islanding operation was introduced in chapter 2. The objective of secondary voltage and frequency controller is to synchronize the voltages and frequency of the terminals of all DGs to reference value dictated by leader DG via the communication matrix by defining the auxiliary control $u_i = Ce_{v_i}$.

e_{v_i} is the local tracking error of the ith DG with respect to the reference signal and neighboring DGs and **C** is controller gain. x_i defined as

$$e_{v_i} = \sum_{j=1}^{N} \zeta_i a_{ij}(x_i - x_j) + g_i \eta_i (x_i - x_{ref}), \tag{4.1}$$

where ζ_i is pinning location and g_i and a_{ij} are pinning gain and communication link gain respectively.

In previous problem formulation, g_i and a_{ij} were considered ideal and constant in all network conditions.

Assumption 1. *The network is connected and symmetric.*

Problem 3. *Let Assumption 1 hold. For any given ζ_i, can one adaptively choose g_i and a_{ij} such that the network in (4.1) asymptotically converges to any given reference value, $\mathbf{x}_{ref}$?*

Control Algorithm

Let us assume the system dynamics to be

$$\dot{x}_i = u_i, \forall i \in \mathcal{N}, \ x_i, u_i \in \mathcal{R}, \tag{4.2}$$

we propose the following adaptive design

$$u_i = \sum_{j=1}^{N} \zeta_i a_{ij}(t)(x_i - x_j) + g_i(t)\eta_i(x_i - x_{ref}), \qquad (4.3)$$

$$\dot{a}_{ij} = 1/2(x_i - x_j)^2, \qquad (4.4)$$

$$\dot{g}_i = \frac{1}{2}\|e_i\| = \frac{1}{2}(x_i - x_{ref})^2, \qquad (4.5)$$

where x_{ref} is the reference trajectory, e_i is the state error,x_i, from reference trajectory, η_i are the pinning location and ζ_i indicates existence of communication link from node j to node i.

Theorem 3. *Give that the network is bidirectional and connected, the system above asymptotically converges to the reference trajectory/state.*

Proof. Let

$$V_i = \frac{1}{2}\sum_{j=1}^{N} e_i{}^2 + \frac{1}{2}\sum_{j=1}^{N} \zeta_i(a_{ij} - \bar{a}_{ij})^2 + \frac{1}{2}\sum_{j=1}^{N} \eta_i(g_i - \bar{g}_i)^2. \qquad (4.6)$$

After taking time derivative of 4.6

$$\dot{V}_i = \sum_{j=1}^{N} e_i\dot{e}_i + \sum_{j=1}^{N} \zeta_i(a_{ij} - \bar{a}_{ij})\dot{a}_{ij} + \sum_{j=1}^{N} \eta_i(g_i - \bar{g}_i)\dot{g}_i, \qquad (4.7)$$

substituting for $\dot{a}_{ij}$ and $\dot{g}_i$

$$\dot{V}_i = -\sum_{i,j\in N} \zeta_i(a_{ij}(t)e_i(e_i - e_j) - \sum_{i\in N}\eta_i g_i e_i^2 + \sum_{i,j\in N}\zeta_i a_{ij}\dot{a}_{ij} - \sum_{i,j\in N}\zeta_i\bar{a}_{ij}\dot{a}_{ij} + \sum_{i\in N}\eta_i g_i\dot{g}_i - \sum_{i\in N}\eta_i\bar{g}_i\dot{g}_i.$$

$$(4.8)$$

Simplification of (4.8) will result in

$$\dot{V}_i = \sum_{i,j \in N} \zeta_{ij} a_{ij} [e_i (e_i - e_j) - \dot{a}_{i,j}] - \sum_{i \in N} \eta_i g_i (e_i^2 - \dot{g}_i) - \sum_{i,j \in N} \zeta_{ij} \bar{a}_{ij} \dot{a}_{ij} - \sum_{i \in N} \eta_{ij} \bar{g}_i \dot{g}_i. \quad (4.9)$$

We know $\dot{g}_i = \|e_i\|^2$; therefore, second term in 4.10 will be eliminated to achieve

$$\dot{V}_i = \sum_{i,j \in N} \zeta_{ij} a_{ij} [e_i (e_i - e_j) - \dot{a}_{i,j}] - \sum_{i,j \in N} \zeta_{ij} \bar{a}_{ij} \dot{a}_{ij} - \sum_{i \in N} \eta_{ij} \bar{g}_i \|e_i\|^2, \quad (4.10)$$

substituting $\dot{a}_{ij} = \frac{1}{2}(e_i - e_j)^2$ will result in

$$\dot{V}_i = -\frac{1}{2} \sum_{i \in N} (\sum_{j \in N} \zeta_{ij} a_{ij}) \|e_i\|^2 + \frac{1}{2} \sum_{j \in N} (\sum_{i \in N} \zeta_{ij} a_{ij}) \|e_j\|^2 - \sum_{i,j \in N} \bar{a}_{ij} \zeta_{ij} \|e_i - e_j\|^2 \sum_{i \in N} \eta_i g_i \|e_i\|^2. \quad (4.11)$$

If the communication matrix is symmetrical /bidirectional then

$$\dot{V}_i = -\sum_{i,j=1^N} \bar{a}_{ij} \zeta_{ij} \|e_i - e_j\|^2 - \sum_{i=1^N} \eta_{ij} \bar{g}_i \|e_i\|^2. \quad (4.12)$$

$\dot{V}_i$ is a negative definite function of the states errors from the reference trajectory if there exist a $\eta_i \neq 0$ for some i

$\exists\, i \ni \eta_i \neq 0\ (\eta_i = 1)$.

Hence

$$\|e_i\| \to 0$$

.   □

Case study

A microgrid in islanded mode with four DGs, corresponding to Fig. 3.8a, is used to verify the performance of the adaptive voltage and frequency control gain strategy. The nominal voltage and frequency are $380V$ and $50\ Hz$., respectively. DGs are connected to each other through three RL lines. The DG, line, and load specifications can be found in the appendix. Based on our proposed intelligent pinning algorithm stated in chapter four, related to Fig. 3.8b, pinning DG2 is the best pinning location. Voltage and frequency profile of microgrid applying adaptive pinning gain control technique is shown in Fig. 4.1.
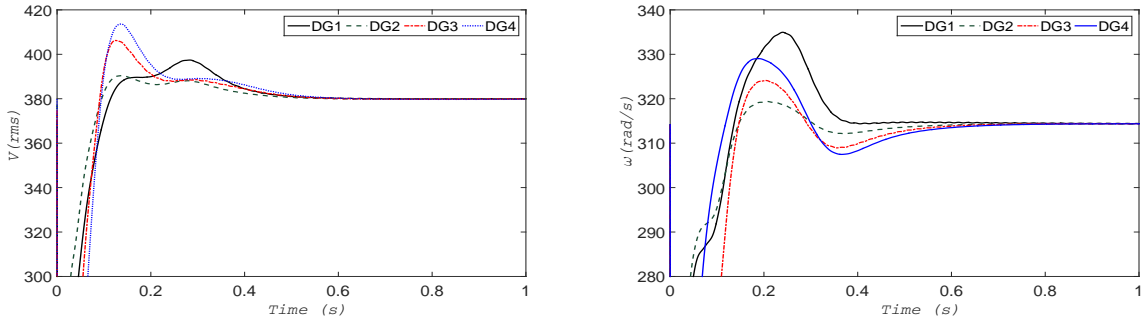
Figure 4.1: DGs terminal amplitudes voltage (at left) and frequency (at right) corresponding to Fig. 3.8 communication network.

Figs. 4.2 and 4.3 are communication link control gains for microgrid lines and pinning control gains for voltage and frequency, respectively. Each communication line has its own communication link gain. As it can be seen, voltage communication link gain control for the line between DG2 and DG3 ,$L23$, settled at 350 while frequency communication link gain reached 250. Our intelligent pinning gain results in chapter four were based on fixed communication links and pinning gain of 400. As indicated in Fig 4.1, adaptive voltage gain controller restores the DGs' voltage amplitude to the reference voltage (380 V) at $t_{sv} = 0.6$ (s) while the microgrid frequency restoration occur at $t_{sf} = 0.8$ (s). In practical, the microgid has few cycles to restore its voltage and frequency to

44

prevent the operation of voltage and frequency relays. The protective power relays' voltage and frequency elements are typically set to $0.88\ (p.u.) \le v_{\mathrm{mag}} \le 1.1\ (p.u.)$ and $295.3(rad/s) \le \omega \le 317.3(rad/s)$ for 10-20 cycles. Results indicated in this case study showed the proposed adaptive frequency control strategy is impractical in microgrid islanding operation since all DGs' output frequency reach under 317.3(rad/s) after 20 cycles. The proposed adaptive voltage gain control can be applied solely since the microgrid is much less sensitive to voltage fluctuation.
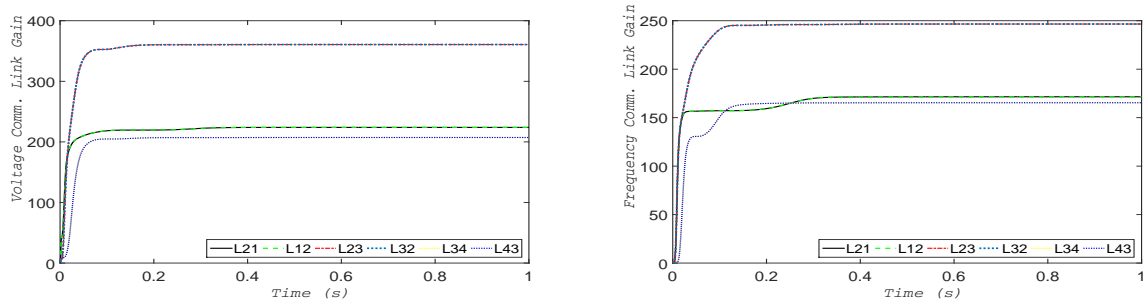
Figure 4.2: Voltage communication link gain (at left) and frequency communication link gain (at right) corresponding to Fig. 3.8 communication network.
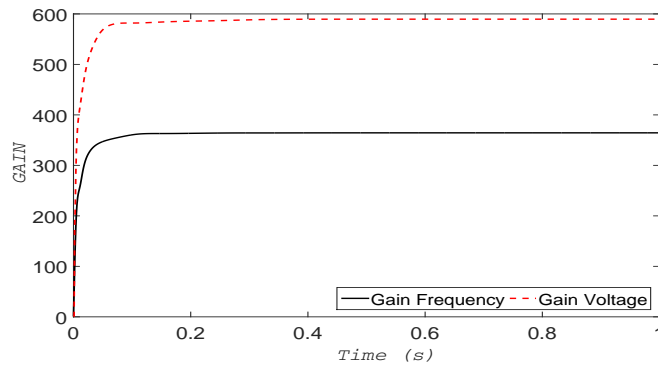
Figure 4.3: Voltage and frequency pinning gain corresponding to Fig. 3.8 communication network.

45

Adaptive secondary control via pinning in medium and low voltage microgrid

The microgrid voltage and frequency regulations are essential for both grid connected and autonomous mode and it can be achieved by using several control techniques either with or without communication signals. In grid connected mode, voltage and frequency are dictated by the main grid while in islanded operation mode, it is necessary to have reference voltage and frequency signals in the distributed generators (DGs) control to regulate both voltage and frequency at all locations [41] [42].

Typical microgrid control hierarchy includes primary and secondary controller. Usually a well-known voltage and frequency droop control technique is applied in the primary controller of the microgrid for deriving the reference signals for the inverter DGs input to ensure active and reactive power sharing [43–48]. Decentralize techniques such as distributed cooperative control as a secondary controller is recently introduced in the microgrid to compensate for voltage and frequency deviations of the DGs from reference value caused by primary controller [49–51]. For microgrid synchronization to reach nominal point, the reference values for voltage and frequency should be provided to the cooperative controller in one or multiple DGs via pinning control technique where a fraction of the DGs in the network have the reference values [27]. Pinning based control for network synchronization based on the simulation results has been studied in [25][27]. Pinning based strategy application in the microgrid autonomous mode using classical droop equation is studied in [37].

Classical droop equation is written based on power flow theory for AC transmission system which is considered mostly an inductive network. In an inductive network, the frequency depends on the active power, while the voltage depends on the reactive power [52–55]. There has been research and studies for the droop technique called opposite droop, written for resistive network where frequency depends on the reactive power while voltage depends on the active power [56–58].

Despite its reputation, classical droop has well known limitations such as poor transient, power sharing accuracy, and output voltage regulation [59]. Accurate active power sharing of the DGs in islanding operation can be usually reached by droop equation. However, the performance of reactive power sharing under droop control may be weakened due to the impact of output line impedance between the DGs and loads which causes an inherent trade-off between power sharing and voltage regulation [60–63]. Several techniques have been proposed to overcome reactive power sharing issues in classical droop equation [60, 64–67]. Classical and opposite droop equations do not completely reflect the line parameters in medium or low voltage microgrid because resistive or inductive parts of the line between sources cannot be neglected. In such situations, there is a coupling between active and reactive power controls. This research considered the general droop equation adopted from [68] in which both R and X parameters of the line are reflected to address the simultaneous impacts of active and reactive power fluctuations on the microgrids voltage and frequency. Based on that we formulate the problem of adaptive distributed cooperative control in the microgrids to overcome the drawback of existing droop based control methods and improve the power sharing and voltage regulation. Our proposed secondary control strategy is adaptive with line parameters and can be applied to all types of microgrids. Flexibility and effectiveness of the proposed control technique are presented in the simulation results for power system topology with different line parameters and communication networks. The DG dynamics in our tracking synchronization problem is adopted from [29] [34].

Preliminaries

Droop Control

The output power flow of the ith inverter shown in Fig. 4.4 can be calculated as:
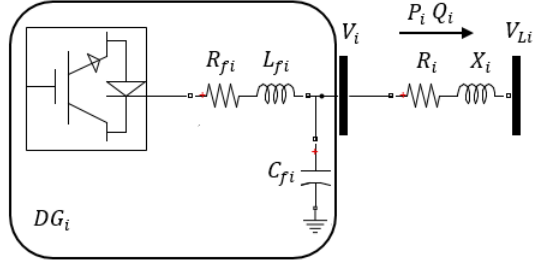
Figure 4.4: Simple DG inverter block connected to the microgrid

$$P_i = \frac{V_i}{R_i^2 + X_i^2}[R_i(V_i - V_{Li}cos\delta_i) + X_iV_{Li}sin\delta_i], \tag{4.13}$$

$$Q_i = \frac{V_i}{R_i^2 + X_i^2}[-R_iV_{Li}sin\delta_i + X_i(V_i - V_{Li}cos\delta_i)]. \tag{4.14}$$

Assuming the transmission line when $X_i \gg R_i$ and small power angle δ_i, 4.13 and 4.14 result in

$$\delta_i = \frac{X_iP_i}{V_iV_{Li}}, \tag{4.15}$$

$$V_i - V_{Li} = \frac{X_iQ_i}{V_i}, \tag{4.16}$$

which shows the dependency of the power angle and inverter output voltage to P and Q, respectively. These conclusions form the basis of the well-known classical frequency and voltage droop regulation through, respectively, active and reactive power.

$$\begin{cases} \omega_i^\star = \omega_{n_i} - m_{P_i}P_i \\ V_{i,mag}^\star = V_{n_i} - n_{Q_i}Q_i, \end{cases} \tag{4.17}$$

where $\omega_i^\star$ and $V_{i,mag}^\star$ are the desired angular frequency and voltage amplitude of the ith DG, respectively; P_i and Q_i are the active and reactive power outputs of the ith DG; ω_{n_i} and V_{n_i} are reference angular frequency and voltage set points determined by the secondary control, respectively; and

m_{P_i} and n_{Q_i} are droop coefficients for real and reactive power.

In the generalized droop equation, R_i, which is the key parameter in medium and low voltage microgrid, is no longer neglected. Considering both R_i and X_i results in the effect of active and reactive power on voltage and frequency regulation. Adopted from [68], modified active and reactive power P'_i and Q'_i are

$$P'_i = \frac{X_i}{Z_i}P_i - \frac{R_i}{Z_i}Q_i, \tag{4.18}$$

$$Q'_i = \frac{R_i}{Z_i}P_i + \frac{X_i}{Z_i}Q_i. \tag{4.19}$$

Substituting 4.18 and 4.19 in 4.15 and 4.16 results in the generalized droop equation

$$\begin{cases} \omega^\star_i - \omega_{n_i} = -m_{P_i}\frac{X_i}{Z_i}P_i + m_{P_i}\frac{R_i}{Z_i}Q_i \\ V^\star_{i,mag} - V_{n_i} = -n_{Q_i}\frac{R_i}{Z}P_i - n_{Q_i}\frac{X_i}{Z_i}Q_i, \end{cases} \tag{4.20}$$

which shows the simultaneous impact of active and reactive power on voltage and frequency regulation.

Inverter Model

The block diagram of voltage source inverter (VSI) based DG with the primary and secondary control was shown in chapter 2, Fig. 2.1. This model consists of three legged inverter bridge connected to DC voltage source such as solar photovoltaic cells. The DC bus dynamics and switching process of the inverter can be neglected due to the assumption of ideal DC source from the DG and realization of high switching frequency of the bridge, respectively [29] [34].

The primary controller of a DG inverter consists of three parts: power, voltage, and current controllers which set the voltage magnitude and frequency of the inverter [34] [35]. As shown in Fig.

2.1, the control process of primary controller is expressed in $d - q$ coordinate system. The objective of the primary controller is to align the output voltage of each DG on $d-$axis to the inverter's reference frame and set the $q-$axis reference to zero.

The instantaneous active and reactive powers of inverter output are passed through low pass filters with cut-off frequency of ω_c to obtain the fundamental component of active and reactive powers: P_i and Q_i. The dynamics of the power controller can be written as

$$\dot{P}_i = -\omega_{c_i} P_i + \omega_{c_i}(v_{od_i} i_{od_i} + v_{oq_i} i_{oq_i}), \tag{4.21}$$

$$\dot{Q}_i = -\omega_{c_i} Q_i + \omega_{c_i}(v_{oq_i} i_{od_i} - v_{od_i} i_{oq_i}). \tag{4.22}$$

Inverter model and specifications were fully covered in chapter 3.

System Model

In general, the droop equations are [68]

$$\omega_i = \omega_{n_i} - m_{Pi}\, \theta_{1i}\, P_i + m_{Pi}\, \theta_{2i}\, Q_i, \tag{4.23}$$

$$V_i = V_{n_i} - n_{Qi}\, \theta_{2i}\, P_i - n_{Qi}\, \theta_{1i} Q_i, \tag{4.24}$$

where $\theta_{1i} \triangleq X_i/Z_i$ and $\theta_{2i} \triangleq R_i/Z_i$.

Assumption 2. *The network is connected and symmetric.*

To properly formulate the control problem, let us define the following variables

$$\theta_{\mathbf{i}} \triangleq [\theta_{1i} \; \theta_{2i}]^T, \qquad\qquad \theta \triangleq [\theta_{\mathbf{1}}^T \; \cdots \; \theta_{\mathbf{N}}^T]^T,$$

$$\mathbf{x}_i \triangleq [\omega_i \; V_i]^T, \qquad\qquad \mathbf{x} \triangleq [\mathbf{x}_1^T \; \cdots \; \mathbf{x}_N^T]^T,$$

$$\mathbf{x}_{n_i} \triangleq [\omega_{n_i} \; V_{n_i}]^T, \qquad\qquad \mathbf{x}_n \triangleq [\mathbf{x}_{n_1}^T \; \cdots \; \mathbf{x}_{n_N}^T]^T,$$

$$\mathbf{W}_i \triangleq \begin{bmatrix} m_i \dot{P}_i & -m_i \dot{Q}_i \\ n_i \dot{Q}_i & n_i \dot{P}_i \end{bmatrix} \qquad \mathbf{W} \triangleq \mathrm{diag}([\mathbf{W}_1 \cdots \mathbf{W}_N]^T).$$

By differentiating from (4.23) and (4.24), we have

$$\dot{\mathbf{x}}_i = \dot{\mathbf{x}}_{n_i} - \mathbf{W}_i \, \theta_i. \qquad\qquad (4.25)$$

Problem 4. *Let Assumption 2 hold. Assume that θ_{ij}'s are constant and unknown, then what is the proper choice of $\mathbf{x}_{n_i}$ such that the network in (4.25) asymptotically converges to any given reference values, $\mathbf{x}_{ref}$?*

Main Results

Since the θ_i is assumed to be unknown/uncertain, in order to achieve synchronization in the network, let

$$\dot{\mathbf{x}}_{n_i} = \mathbf{u}_i + \mathbf{W}_i \, \hat{\theta}_i, \qquad\qquad (4.26)$$

where $\hat{\theta}_i$ is the estimate of θ_i and will be derived later. Substituting (4.26) in (4.25), we have

$$\dot{\mathbf{x}}_i = \mathbf{ui} - \mathbf{W_i}(\theta_i - \hat{\theta}_i). \tag{4.27}$$

If the θ_i's are correctly estimated, then cooperative control law to achieve synchronization to reference signal can be chosen as

$$\mathbf{u}_i = \sum_{j=1}^{N} a_{ij}\mathbf{C}(\mathbf{x}_j - \mathbf{x}_i) + g_i\zeta_i\mathbf{C}(\mathbf{x}_{\text{ref}} - \mathbf{x}_i), \tag{4.28}$$

where $\mathbf{C} \triangleq \text{diag}([c_\omega\ c_V])$ are the controller gains. If we let $\mathbf{u} \triangleq [\mathbf{u}_1^T \cdots \mathbf{u}_N^T]^T$, then we have

$$\mathbf{u} = -[(\mathbf{L} + \mathbf{GZ}) \otimes \mathbf{C}](\mathbf{x} - \mathbf{1}_N \otimes \mathbf{x}_{\text{ref}}). \tag{4.29}$$

Hence, the dynamic of the network, can be written as

$$\dot{\mathbf{e}} = -[(\mathbf{L} + \mathbf{GZ}) \otimes \mathbf{C}]\mathbf{e} - \mathbf{W}(\theta - \hat{\theta}), \tag{4.30}$$

where $\mathbf{e} \triangleq \mathbf{x} - \mathbf{1}_N \otimes \mathbf{x}_{\text{ref}}$ is the synchronization error.

Theorem 4. *If Assumption 2 holds and there exists at least $\zeta_i = 1$, then the network with input*

$$\dot{\mathbf{x}}_{n_i} = -\sum_{j=1}^{N} a_{ij}\mathbf{C}(\mathbf{x}_i - \mathbf{x}_j) - g_i\zeta_i\mathbf{C}(\mathbf{x}_i - \mathbf{x}_{ref}) + \mathbf{W}_i\hat{\boldsymbol{\theta}}_i, \tag{4.31}$$

$$\dot{\hat{\boldsymbol{\theta}}}_i = -k_i\mathbf{W}_i^T\sum_{j=1}^{N} a_{ij}\mathbf{C}\,(\mathbf{x}_i - \mathbf{x}_j) - k_i\mathbf{W}_i^T g_i\zeta_i\mathbf{C}\,(\mathbf{x}_i - \mathbf{x}_{ref}) \quad \forall k_i,\ g_i > 0, \tag{4.32}$$

asymptotically converges to $\mathbf{x}_{ref}$.

Proof. Consider the following Lyapunov function

$$V = \frac{1}{2}\mathbf{e}^T \mathbf{P} \mathbf{e} + \sum_{i=1}^{N} \frac{1}{2k_i}(\theta_i - \hat{\theta}_i)^T(\theta_i - \hat{\theta}_i), \qquad (4.33)$$

where $\mathbf{P}$ is some symmetric positive definite matrix. Differentiating from equation above, we have

$$\dot{V} = \mathbf{e}^T \mathbf{P}$$

$$\dot{V} = -\mathbf{e}^T \mathbf{P} \Big((\mathbf{L} + \mathbf{G}\,\mathbf{Z}) \otimes \mathbf{C} \Big) \mathbf{e}. \qquad (4.34)$$

It is known if Assumption 2 holds and there exits at least one $\zeta_i = 1$, then $(\mathbf{L} + \mathbf{G}\,\mathbf{Z}) \otimes \mathbf{C}$ is a symmetric positive definite matrix, consequently, $\mathbf{P}\Big((\mathbf{L} + \mathbf{G}\,\mathbf{Z}) \otimes \mathbf{C} \Big)$ is positive definite[1], by using Barbalet's Lemma, we can conclude that

$$\lim_{t\to\infty} \mathbf{e}^T \mathbf{P} \Big((\mathbf{L} + \mathbf{G}\,\mathbf{Z}) \otimes \mathbf{C} \Big) \mathbf{e} = 0 \quad \Rightarrow \quad \lim_{t\to\infty} \mathbf{e} = \mathbf{0},$$

which proves that $\mathbf{x}_i$ asymptotically converge to $\mathbf{x}_{\text{ref}}$.

Although this analysis is true for any symmetric positive definite matrix $\mathbf{P}$, however, as $\mathbf{x}_{\text{ref}}$ is not available in all the nodes, for any arbitrary symmetric positive definite $\mathbf{P}$, does not lead to an implementable estimation/adaptation of θ_i's. One candidate matrix for $\mathbf{P}$ is $(\mathbf{L} + \mathbf{G}\,\mathbf{Z}) \otimes \mathbf{C}$, where we have

$$\mathbf{W}\Big(\mathbf{L} + \mathbf{G}\,\mathbf{Z}) \otimes \mathbf{C} \Big)\mathbf{e} = \mathbf{W}\Big(\mathbf{L} \otimes \mathbf{C} \Big)\mathbf{e} + \mathbf{W}\Big((\mathbf{G}\,\mathbf{Z}) \otimes \mathbf{C} \Big)\mathbf{e}$$

$$= \mathbf{W}\Big(\mathbf{L} \otimes \mathbf{C} \Big)\mathbf{x} + \mathbf{W}\Big((\mathbf{G}\,\mathbf{Z}) \otimes \mathbf{C} \Big)(\mathbf{x} - \mathbf{1} \otimes \mathbf{x}_{\text{ref}}), \qquad (4.35)$$

---

[1]Product of two symmetric positive definite matrices are positive definite, this can be easily shown by Weyl's inequalities for product .

which requires the knowledge of x_{ref} only on the pinning location(s). □

In summary the reference in droop equations, namely, ω_{n_i} and V_{n_i} are set by the following set of equations.

Case 1: No power sharing

In the non power sharing scheme, there is no real power control for DGs' output power. DGs will inject active power based on their droop coefficient and maximum allowable power limit. This scheme may cause the increasing the power losses in the microgrid autonomus mode. The reference signals, ω_{n_i} and V_{n_i}, set by

$$\omega_{n_i} = -\int \left[\sum_{j=1}^{N} a_{ij}(\omega_i - \omega_j) + g_i\zeta_i(\omega_i - \omega_{\text{ref}}) - m_i\hat{\theta}_{1i}\dot{P}_i + m_i\dot{Q}_i\hat{\theta}_{2i} \right] dt,$$

$$V_{n_i} = -\int \left[\sum_{j=1}^{N} a_{ij}(V_i - V_j) + g_i\zeta_i(V_i - V_{\text{ref}}) - n_i\hat{\theta}_{2i}\dot{P}_i - n_i\dot{Q}_i\hat{\theta}_{1i} \right] dt,$$

$$\dot{\hat{\theta}}_{1i} = -k_i \left(c_\omega m_i\dot{P}_i \sum_{j=1}^{N} a_{ij}(\omega_i - \omega_j) + c_\omega m_i\dot{P}_i g_i\zeta_i(\omega_i - \omega_{\text{ref}}) \right.$$

$$\left. + c_v n_i\dot{Q}_i \sum_{j=1}^{N} a_{ij}(V_i - V_j) + c_v n_i\dot{Q}_i g_i\zeta_i(V_i - V_{\text{ref}}) \right),$$

$$\dot{\hat{\theta}}_{2i} = -k_i \left(-c_\omega m_i\dot{Q}_i \sum_{j=1}^{N} a_{ij}(\omega_i - \omega_j) - c_\omega m_i\dot{Q}_i g_i\zeta_i(\omega_i - \omega_{\text{ref}}) \right.$$

$$\left. + c_v n_i\dot{P}_i \sum_{j=1}^{N} a_{ij}(V_i - V_j) + c_v n_i\dot{P}_i g_i\zeta_i(V_i - V_{\text{ref}}) \right).$$

where the dynamics of $\dot{P}_i$ and $\dot{Q}_i$ are given in (4.21) and (4.22) respectively.

Case 2: Power sharing based on frequency droop

The power sharing method is proposed since the frequency of the microgrid freely fluctuates when

none of the DG units are able to enforce the base frequency during an autonomous mode. In this method, the load demand is shared among the DG units proportional to the active power rating of units. The reference signals, ω_{n_i} and V_{n_i}, set by

$$\omega_{n_i} = -\int \left[\sum_{j=1}^{N} a_{ij}(\omega_i - \omega_j) + g_i\zeta_i(\omega_i - \omega_{\text{ref}}) - m_i\dot{P}_i\hat{\theta}_{1i} + m_i\dot{Q}_i\hat{\theta}_{2i} \right] dt,$$

$$V_{n_i} = -\int \left[\sum_{j=1}^{N} a_{ij}(V_i - V_j) + g_i\zeta_i(V_i - V_{\text{ref}}) - n_i\dot{P}_i\hat{\theta}_{2i} - n_i\dot{Q}_i\hat{\theta}_{1i} \right] dt,$$

$$\dot{\hat{\theta}}_{1i} = -k_i \left(c_\omega\, m_i\dot{P}_i \sum_{j=1}^{N} a_{ij}(\omega_i - \omega_j) + c_\omega\, m_i\dot{P}_ig_i\zeta_i(\omega_i - \omega_{\text{ref}}) \right.$$

$$\left. + c_v n_i\dot{Q}_i \sum_{j=1}^{N} a_{ij}(V_i - V_j) + c_v n_i\dot{Q}_ig_i\zeta_i(V_i - V_{\text{ref}}) \right),$$

$$\dot{\hat{\theta}}_{2i} = -k_i \left(-c_\omega\, m_i\dot{Q}_i \sum_{j=1}^{N} a_{ij}(\omega_i - \omega_j) - c_\omega\, m_i\dot{Q}_ig_i\zeta_i(\omega_i - \omega_{\text{ref}}) \right.$$

$$\left. + c_v n_i\dot{P}_i \sum_{j=1}^{N} a_{ij}(V_i - V_j) + c_v n_i\dot{P}_ig_i\zeta_i(V_i - V_{\text{ref}}) \right),$$

where the dynamics of $\dot{Q}_i$ is given in (4.22) and dynamics of $\dot{P}_i$ can be calculated as

$$\dot{P}_i = -\frac{c_p}{m_i} \sum_{j=1}^{N} a_{ij} \left(m_i\, P_i - m_j\, P_j \right).$$

Numerical Example/ Case Study

The proposed control methodology is verified with Simpower System Toolbox in MATLAB/Simulink. The microgrid consists of four DGs and it operates on a 3-phase, 380V(L-L) and frequency of 50 Hz ($\omega_0 = 314.15(rad/s)$). DGs are connected through resistance dominated RL branches to re-flect the distribution network and loads are constant . The cut-off frequency of power controller is set to 10% of nominal angular frequency of $\omega_0 = 314.15(rad/s)$. The value chosen for the PI

controllers for voltage and current control loops of each DG, K_{pvi}, K_{VI_i}, K_{PC_i}, K_{IC_i}, are given in Table 4.1. The controller gains c_v and c_ω and pinning gain g are all set to 400, 500 and 1 respectively. The network parameters, the specifications of DGs, and loads are given in Table 4.1.

Table 4.1: Microgrid Test System Specifications

		DG1 and DG2		DG3 and DG4	
DGs		m_p	9.4×10^{-5}	m_p	12.5×10^{-5}
		n_Q	1.3×10^{-3}	n_Q	1.5×10^{-3}
		R_c	$0.03\ \Omega$	R_c	$0.03\ \Omega$
		L_c	$0.35\ mH$	L_c	$0.35\ mH$
		R_f	$0.1\ \Omega$	R_f	$0.1\ \Omega$
		L_f	$1.35\ mH$	L_f	$1.35\ mH$
		C_f	$50\ \mu F$	C_f	$50\ \mu F$
		K_{PV}	1	K_{PV}	1
		K_{IV}	4	K_{IV}	4
		K_{PC}	5	K_{PC}	5
		K_{IC}	40	K_{IC}	40
Loads		Load1		Load2	
		P_{L1}	$12\ KW$	P_{L2}	$12\ KW$
		Q_{L1}	$12\ KVAR$	Q_{L2}	$12\ KVAR$
Lines		L_{12}		L_{23}		L_{34}	
		R_{12}	$0.1\ \Omega$	R_{23}	$0.1\ \Omega$	R_{34}	$0.1\ \Omega$
		X_{12}	$0.1\ \Omega$	X_{23}	$0.1\ \Omega$	X_{34}	$0.1\ \Omega$

To ensure that the proposed control strategy is able to obtain voltage and frequency stability in inductive, resistive and all types of microgrid, simulations have been done in states of $\frac{R}{X} = 1$, $\frac{R}{X} = 10$, and $\frac{R}{X} = 0.1$ for the network configuration of Fig. 3.8a. In this configuration, it is assumed that the DGs communicate with each other through a fixed communication network and only communicate with their neighboring DG. In all cases of line parameters , the microgrid's main breaker opens at $t = 0$ (s) and it goes to the islanding mode while at the same time the secondary adaptive voltage and frequency control are initiated. DGs terminal voltage amplitude and frequency for microgrid with different line parameters for non power sharing case are shown in

Fig. 4.5, 4.6, and 4.7. Based on the adaptive control strategy, it can be seen that all DGs' terminal voltage and frequency return to the reference value dictated by the leader DG.

Figure 4.5: DGs terminal amplitudes voltage (at left) and frequency (at right) corresponding to microgrid with $\frac{R}{X} = 1$.
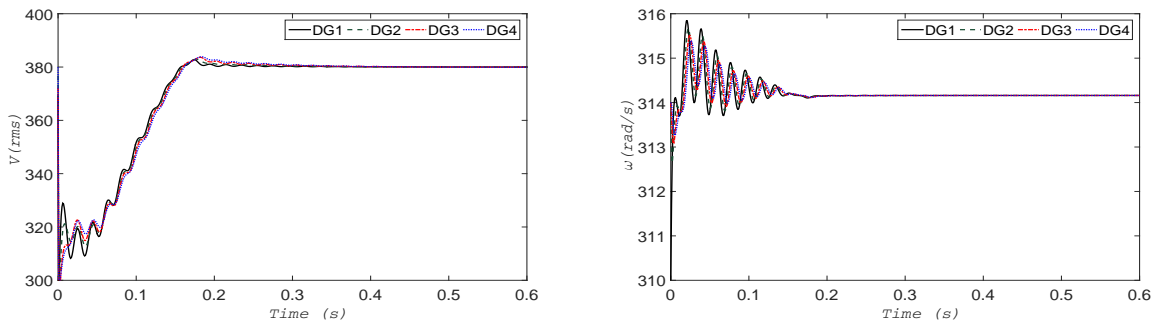
Figure 4.6: DGs terminal amplitudes voltage (at left) and frequency (at right) corresponding to microgrid with $\frac{R}{X} = 10$.

Voltage and frequency regulations of the islanded microgrid based on an adaptive secondary control using generalized droop equation was proposed. In contrast, with existing secondary control techniques using the classical droop, our proposed secondary control strategy is adaptive with line parameters and can be applied to all types of microgrids. Simulation results have been presented to validate the proposed control scheme, showing voltage and frequency regulation of islanded microgrid when the network is resistive, inductive, or unbalanced resistive/inductive.
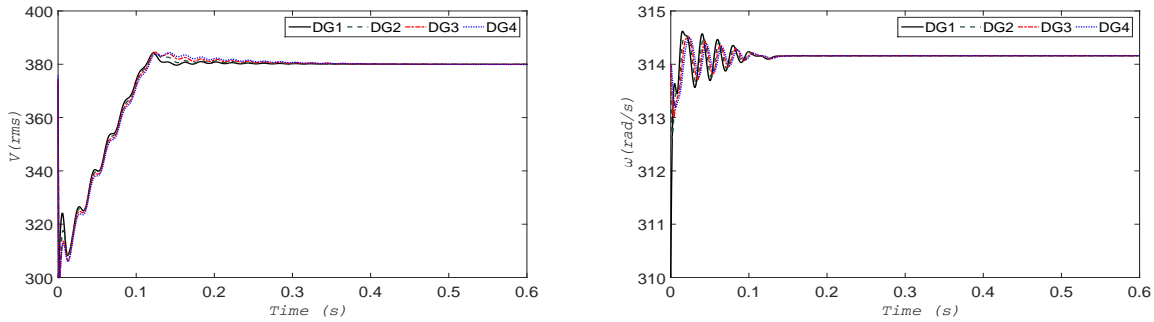
Figure 4.7: DGs terminal amplitudes voltage (at left) and frequency (at right) corresponding to microgrid $\frac{R}{X} = 0.1$.

CHAPTER 5: MICROGRID PROTECTION
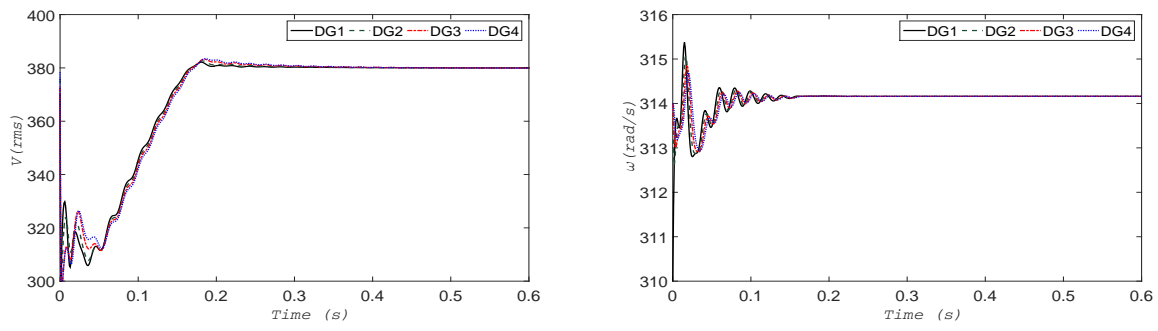
The trustworthy issue of the power system is of great crisis towards both human being's and industrial civilization. In order to secure the power system, numerous meters are deployed through power grids, including interconnected generation plants, transmission lines, transformers and loads, to attain updated state information. These information will be provided to the control center or energy management system (i.e. EMS) and analyzed for the prevention from unreliable factors. Most of unreliability accounts for the false date injection, which is usually induced by adversary or hardware failure. The reliability level of system will be tremendously compromised if such injection is not identified and accumulated, especially when it is maliciously initiated by adversary [69] [70]. In this respect, research on the power system's protection and identification scheme from malicious data injection is of theoretical and practical interest.

Cyber-physical data attack attempts to deviate the accurate data by introducing erroneous value into certain state variable. Intuitively, such injection is able to be identified by comparing the current state with the outcome of distributed estimation of overall power grid [69] [71] [72]. The results merely demonstrated that this detection scheme can identify attacks initiated by random phenomena, such as measurement noise, hardware failure or structure error. Recent research [70] indicated a certain type of attack vector, under which the ordinary residual-based scheme is rendered impotent. Apparently, adversary successfully exploits the measurement matrix and manipulates the state variables with malicious data injection composed by a combination of vectors in the null space of $P - I$. In this case, the residual remains unchanged, which fails ordinary bad data detection (BDD). Further, the vulnerability of large-scale power system to malicious data injection can not be omitted due to the significant financial impact of such stealth attack on electricity market [73]. To this end, a greedy algorithm based protection scheme was proposed in [74], which aims at deploying necessary amount secure meters at key buses to ensure a reliable estimation and evade injection.

Similar work was introduced in [75] and [77], which illustrates how to secure a state estimator from such injection by encrypting a sufficient/minimum number of meters. The protection strategy of [70] is extended further using a polynomial-time algorithm in [76]. A generalized likelihood ratio detection scheme (via convex optimization) is introduced to defense such attack. In addition, several countermeasures to these attacks were also proposed, from additional protected measuring devices [78], to the implementation of improved BDD schemes [70]. Methods to efficiently rank the measurements in terms of their vulnerability and finding sparse attacks requiring the corruption of a low number of measurements were also proposed in [78], [79], and [80]. In [81], a concept of load redistribution (LR) attacks, a special type of false data injection attacks, was introduced and analyzed regarding their damage to power system operation in different time steps with different attacking resource limitations.

From the power system's point of view, the solutions mentioned above are surely functional but they might be too expensive and not be physically practical for expansive distributed network. An enhanced protection scheme against malicious false data injection is proposed. An algebraic criterion is derived to ensure a trustworthy power system against malicious cyber-physical data attacks. The proposed protection scheme takes advantage of expansive nature of power grids, reconfigures its subsystem data structure deterministically, and makes it impossible to organize a successful injection. The identification scheme for finding meters being attacked is proposed as well. Then, analysis can be further performed to remove the sources of malicious data injection.

Preliminary Results

State Estimation

The state estimation problem in power systems is to determine the power system state variables such as voltage angles and magnitudes at all system buses based on the meter measurements. Given that the general measurement function for the power system is

$$z = h(x) + e, \tag{5.1}$$

where $x \in \mathbb{R}^n$ is the overall state vector, $z \in \mathbb{R}^m$ is the overall measurement vector and usually $m > n$, $h(x)$ is the nonlinear function derived from the power flow equations of the overall power grid, and $e \in \mathbb{R}^m$ represents the measurement noise whose covariance matrix is R. It is assumed that the system (5.1) is observable that is a very well-established hypothesis for any centralized algorithm of state estimation. The linearized model of the measurement function (5.1) at time k is

$$z(k) = H(k)x(k) + e(k) \tag{5.2}$$

with a full-rank observation matrix H as $rank(H) = n$, where $rank(\cdot)$ denotes the rank of matrix. The state estimation problem under the assumption of global observability can be formulated with standard WLS which is given by [82]

$$\hat{x}(k+1) = \hat{x}(k) + K(k)H^T(k)R^{-1}(k)\left[z(k) - H(k)\hat{x}(k)\right], \tag{5.3}$$

where $\hat{x}$ is the estimate of state and $K(k) = \left[H^T(k)R^{-1}(k)H(k)\right]^{-1}$ is the error covariance.

Bad Data Detection

With the estimated state vector $\hat{x}$ obtained by state estimation algorithm (5.3), a common approach to verify the integrity of state vector is by computing the $\mathcal{L} - norm$ of measurement residual (i.e. difference between the measurement vector and estimated vector)

$$E \overset{\triangle}{=} \|z - H\hat{x}\|. \tag{5.4}$$

A threshold C_T is pre-defined to control the tolerance of residuals in terms of accuracy of state estimation. If measurement residual is greater than the threshold value, i.e., $E > C_T$, the measurement vector z has a bad data and the state estimation algorithm is not convergent due to either significant measurement/computation errors or gross false data injections. Accordingly, analysis can be performed to position where errors occurs and isolate the suspicious data sources.

Existence of Malicious Data Attacks

In the case that an adversary has access to whole information of H, he is able to launch a malicious attack to the system such that the resulting corrupted state can avoid being detected by the residual test in the sense that $E < C_T$ or $E \approx 0$. Following lemma shows how the adversary chooses such a 'stealth' attack which is summarized in [70].

Lemma 2.1: ([70]) Let $z_a \in \mathbb{R}^m$ be amended coordinated attack vector, which will be injected to original measurement vector z in observation equation (5.2). $z_a = Hc$ where c is the corrupted state induced by the attack vector z_a. Let $P = H \left(H^T H\right)^{-1} H^T$, where P is the projection of observation matrix $H \in \mathbb{R}^{m \times n}$ and clearly $PH = H$. All possible choices of coordinated attack vector $z_a \in \mathbb{R}^m$ lie in the null space of matrix $(P - I)$, that is, $(P - I)z_a = \mathbf{0}$.

According to *Lemma 2.1*, the dimension of null space of matrix $(P-I)$ is n regarding the available measurements in power grid. Note that in the power system, it is typical that the number of meters m (both essential and redundant measurements) are greater than number of state variables n. The coordinated attack vectors z_a always exists if the adversary can get access to all meters' data, power network topology and line data of subsystem to construct H. The attack vectors can be chosen to be a linear combination of the vectors in the null space of $(P-I)$. Secure meters' placement can be considered as one methodology for preventing those coordinated attack vectors and maintaining the subsystem in normal status. However, it could be expensive and physically impractical in expansive distribution network.

Problem Formulation

A power system consists of electric generators, transmission lines, and transformers that form an electrical network. We consider a power system whose electric power grid can be partitioned into a group of ℓ subsystems (shown in figure 5.1). Monitoring the power flow and voltage of each subsystem is important in maintaining system reliability. It is assumed that the subsystem has the capability of reconfiguring its information structure, performing state estimation, and reporting its findings to the upper-level EMS (energy management system).
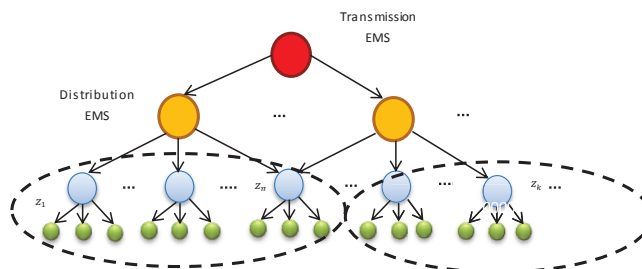
Figure 5.1: Rationale of Protection of Power Systems against Malicious Cyber-Physical Data Attack

In the customary case of state estimation, it is common to find the observation matrix H for the subsystem to estimate the state variables. Hence, if the adversary is capable of getting access to information structure, he always can easily fake the eigen-structure of matrix $[P - I]$ and attempt to corrupt the state vector by a stealth false data injection without being detected by the ordinary BDDs according to the *Lemma 2.1*. Obviously, the counter measurement method is secure meters' placement at sufficient number of locations to prevent measurements being manipulated by adversary. Such an approach would work well for certain size of transmission networks but not for expansive distribution networks.

As an alternative solution, algebraic conditions are proposed in the following section to secure the power system against malicious data attacks.

<div align="center">Protection</div>

<div align="center">*Strategy I*</div>

Partitioning observation matrix H to two separate sub-matrices H_a and H_b as depicted in figure 5.2.

Proposition 3.1: Consider the power system with observation eq. (5.2), the power system is considered secured from malicious data attacks if the observation matrix H can be reconfigured by $\begin{bmatrix} H_a \\ H_b \end{bmatrix}$ where H_a and H_b are full rank and partitioned by two parts, $H_1 = \begin{bmatrix} H_a \\ 0 \end{bmatrix}$ and $H_2 = \begin{bmatrix} 0 \\ H_b \end{bmatrix}$, such that

$$rank \begin{bmatrix} P_1 - I \\ P_2 - I \end{bmatrix} = m, \tag{5.5}$$

where P_1 and P_2 is the projection matrix of H_1 and H_2, respectively.
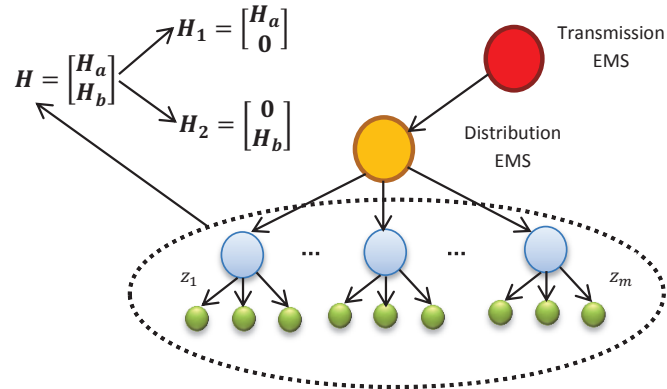
Figure 5.2: Rationale of Protection of Power Systems against Malicious Cyber-Physical Data Attack

The second strategy has defined with having common information in two batches of data H_1 and H_2.

Strategy II

Partitioning observation matrix H to three separate sub-matrices H_a, H_b and H_c as depicted in figure 5.3.

Proposition 3.2: Under scenario above, the power system is considered secured from malicious data attacks if the observation matrix H can be reconfigured by $\begin{bmatrix} H_a \\ H_b \\ H_c \end{bmatrix}$ and partitioned by two parts,

$$H_1 = \begin{bmatrix} H_a \\ H_b \\ 0 \end{bmatrix} \text{ and } H_2 = \begin{bmatrix} 0 \\ H_b \\ H_c \end{bmatrix}, \text{ such that}$$

$$rank \begin{bmatrix} P_1 - I \\ P_2 - I \end{bmatrix} = m, \tag{5.6}$$

where P_1 and P_2 is the projection matrix of H_1 and H_2, respectively.
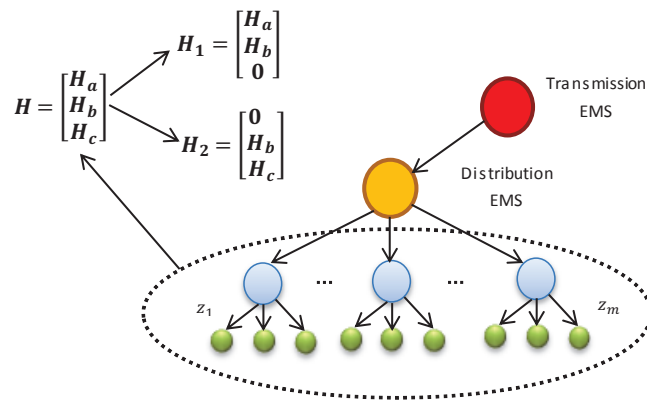
Figure 5.3: Rationale of Protection of Power Systems against Malicious Cyber-Physical Data Attack

Proof: It is straightforward to see that, under condition (5.5,5.6), the only admissible solution of attack vector is $z_a = 0$. In other words, any attack vector rather than $\mathbf{0}$ yields a non-zero residual even if the adversary knows H precisely. ∎

It is worthy to note that the proposed method is employing reconfiguration of observation matrix to secure the power system from any attack, and it works as long as the power system has sufficient redundancy to ensure the observability for the sub-areas represented by H_1 and H_2. The proof for

the feasibility of finding sub-matrices H_1 and H_2 will be provided in the next section.

Main Results

In this section, we will first present the feasibility of finding sub-matrices H_1 and H_2 for H in both strategies, and then the protection and identification schemes for power systems against malicious data attacks.

Recall the property of Idempotent Matrix in [83], it is straightforward to see that P_1 and P_2 are both idempotent. Thus, $I - P_1$ and $I - P_2$ are idempotent as well. Let us define $A = P_1 - I$ and $C = P_2 - I$, then the following facts are obvious:

Fact 4.1: $-A$ and $-C$ are idempotent. Also,

$$A^2 = -A, C^2 = -C, (-A)^\sharp = -A, \tag{5.7}$$

where $\sharp$ denotes the generalized inverse of a matrix.

Fact 4.2: P_1 is the projection matrix of H_1,

$$trace(P_1) = rank(P_1) = rank(H_1) \tag{5.8}$$

where $trace(\cdot)$ denotes the trace of a matrix.

Based on the above facts, we have the following proposition.

Proposition 4.3: $rank(A) = m - n$ if $rank(H_1) = n$. **Proof:** With *Fact 4.2*

$$\begin{aligned}
rank(A) &= rank(P_1 - I) = rank(I - P_1) \\
&= trace(I - P_1) = trace(I) - trace(P_1) \\
&= m - rank(H_1) = m - n,
\end{aligned} \tag{5.9}$$

if H_1 is observable to the entire system, which means $rank(H_1) = n$. ∎

The following lemma will be used for the main result as well.

Lemma 4.4: ([84]) Let $A \in \mathbb{C}^{m \times n}$, $B \in \mathbb{C}^{m \times k}$, $C \in \mathbb{C}^{l \times n}$ and $D \in \mathbb{C}^{l \times k}$. Then,

$$\begin{aligned}
rank([A, B]) &= rank(A) + rank(B - AA^\sharp B) \\
&= rank(B) + rank(A - BB^\sharp A) \\
rank(\begin{bmatrix} A \\ C \end{bmatrix}) &= rank(A) + rank(C - CA^\sharp A) \\
&= rank(C) + rank(A - AC^\sharp C) \\
rank(\begin{bmatrix} A & B \\ C & 0 \end{bmatrix}) &= rank(B) + rank(C) \\
&\quad + rank[(I_m - BB^\sharp)A(I_n - C^\sharp C)] \\
rank(\begin{bmatrix} A & B \\ C & D \end{bmatrix}) &= rank(A) \\
&\quad + rank(\begin{bmatrix} 0 & B - AA^\sharp B \\ C - CA^\sharp A & D - CA^\sharp B \end{bmatrix}).
\end{aligned} \tag{5.10}$$

Then, we are ready to present the first main result as follows.

68

Theorem 4.5: Given $H = \begin{bmatrix} H_a \in \mathbb{R}^{l \times n} \\ H_b \in \mathbb{R}^{m-l \times n} \end{bmatrix}$, $rank \begin{bmatrix} P_1 - I \\ P_2 - I \end{bmatrix} = m$ holds if $H_1 = \begin{bmatrix} H_a \\ 0 \end{bmatrix}$, $H_2 = \begin{bmatrix} 0 \\ H_b \end{bmatrix}$, and $rank(H_1) = rank(H_2) = n$.

Proof: Recall second equation of (9) in *Lemma 4.4*,

$$rank(\begin{bmatrix} A \\ C \end{bmatrix}) = rank(A) + rank(C - CA^\sharp A)$$

$$= m - n + rank(C - CA^\sharp A)$$

(5.11)

due to *Proposition 4.3*, which requires $rank(H_1) = rank(H_a) = n$.
Given $H_1 = \begin{bmatrix} H_a \\ 0 \end{bmatrix}$,

$$P_1 = H_1(H_1^T H_1)^{-1} H_1^T = \begin{bmatrix} H_a(H_a^T H_a)^{-1} H_a^T & 0 \\ 0 & 0 \end{bmatrix},$$

(5.12)

and $H_2 = \begin{bmatrix} 0 \\ H_b \end{bmatrix}$,

$$P_2 = H_2(H_2^T H_2)^{-1} H_2^T = \begin{bmatrix} 0 & 0 \\ 0 & H_b(H_b^T H_b)^{-1} H_b^T \end{bmatrix}.$$

(5.13)

Then, with *Fact 4.1*,

$$C - CA^\sharp A = C(I - A^\sharp A) = C(I - A^2)$$

$$= C(I + A) = CP_1$$

$$= \begin{bmatrix} -I & 0 \\ 0 & H_b(H_b^T H_b)^{-1}H_b^T - I \end{bmatrix}$$

$$\cdot \begin{bmatrix} H_a(H_a^T H_a)^{-1}H_a^T & 0 \\ 0 & 0 \end{bmatrix}$$

$$= \begin{bmatrix} -H_a(H_a^T H_a)^{-1}H_a^T & 0 \\ 0 & 0 \end{bmatrix}$$

(5.14)

Thus,

$$rank(C - CA^\sharp A) = rank(H_a) = rank(H_1).$$

(5.15)

It finalizes the proof by also noticing that both H_1 and H_2 are required to be full rank n. ∎

Theorem 4.6: Given $H = \begin{bmatrix} H_a \in \mathbb{R}^{l \times n} \\ H_b \in \mathbb{R}^{k \times n} \\ H_c \in \mathbb{R}^{m-l-k \times n} \end{bmatrix}$, $rank \begin{bmatrix} P_1 - I \\ P_2 - I \end{bmatrix} = m$ holds if $H_1 = \begin{bmatrix} H_a \\ H_b \\ 0 \end{bmatrix}$,

$H_2 = \begin{bmatrix} 0 \\ H_b \\ H_c \end{bmatrix}$, and one of four conditions below satisfies:

$rank(H_a) = rank \begin{bmatrix} H_b \\ H_c \end{bmatrix} = n, rank(H_c) = rank \begin{bmatrix} H_a \\ H_b \end{bmatrix} = n,$

$rank(H_b) = rank \begin{bmatrix} H_a \\ H_c \end{bmatrix} = n$,and

$rank(H_a^T H_a + H_b^T H_b \hat{H} H_c^T H_c) = n$, where

$\hat{H} = (H_b^T H_b + H_c^T H_c)^{-1}$.

Proof:Again, recall second equation of (9) in *Lemma 4.4* then,

$$rank(\begin{bmatrix} P_1 - I \\ P_2 - I \end{bmatrix}) = rank(P_1 - I) + rank((P_2 - I) - \\ (P_2 - I)(P_1 - I)^{\sharp}(P_1 - I))$$ (5.16)

$$= m - n + rank((P_2 - I)P_1)$$

due to *Proposition 4.3*, which requires $rank((P_2 - I)P_1) = n$.

Given $H_1 = \begin{bmatrix} H_a \\ H_b \\ 0 \end{bmatrix}$ and $H_2 = \begin{bmatrix} 0 \\ H_b \\ H_c \end{bmatrix}$,

$$(P_2 - I)P_1 = \\ \begin{bmatrix} -H_a \tilde{H} H_a^T & -H_a \tilde{H} H_b^T & 0 \\ H_b \hat{H} H_b^T H_b \tilde{H} H_a^T - H_b \tilde{H} H_a^T & H_b \hat{H} H_b^T H_b \tilde{H} H_b^T - H_b \tilde{H} H_b^T & 0 \\ H_c \hat{H} H_b^T H_b \tilde{H} H_a^T & H_c \hat{H} H_b^T H_b \tilde{H} H_b^T & 0 \end{bmatrix},$$ (5.17)

where

$\hat{H} = (H_b^T H_b + H_c^T H_c)^{-1}$ and $\tilde{H} = (H_a^T H_a + H_b^T H_b)^{-1}$.

$$rank((P_2 - I)P_1)$$

$$= rank(\begin{bmatrix} -H_a \\ H_b\hat{H}H_b^T H_b - H_b \\ H_c\hat{H}H_b^T H_b \end{bmatrix} \begin{bmatrix} \tilde{H}H_a^T & \tilde{H}H_b^T & 0 \end{bmatrix}) \tag{5.18}$$

$$= rank(\begin{bmatrix} -H_a \\ H_b\hat{H}H_b^T H_b - H_b \\ H_c\hat{H}H_b^T H_b \end{bmatrix}) = rank(\begin{bmatrix} -H_a \\ -H_b\hat{H}H_c^T H_c \\ H_c\hat{H}H_b^T H_b \end{bmatrix})$$

due to $rank(\begin{bmatrix} \tilde{H}H_a^T & \tilde{H}H_b^T & 0 \end{bmatrix}) = n$ since $\tilde{H}$ and H_1 are with full rank n.

Lemma 1: If the $rank(H_a) = n$ then $rank(\begin{bmatrix} H_a \\ H_b\hat{H}H_c^T H_c \\ H_c\hat{H}H_b^T H_b \end{bmatrix}) = n$ and with noticing that $rank(\begin{bmatrix} 0 \\ H_b \\ H_c \end{bmatrix}) = n$, It finalize the proof. The proof of second and third condition can be shown in the same way.

Lemma 2: If $rank(H_a) \neq n$, then $rank(\begin{bmatrix} -H_a \\ -H_b\hat{H}H_c^T H_c \\ H_c\hat{H}H_b^T H_b \end{bmatrix})$

$$= rank(\begin{bmatrix} -H_a^T & -H_c^T H_c\hat{H}H_b^T & H_b^T H_b\hat{H}H_c^T \end{bmatrix} \begin{bmatrix} -H_a \\ -H_b\hat{H}H_c^T H_c \\ H_c\hat{H}H_b^T H_b \end{bmatrix})$$

$$= rank(\begin{bmatrix} H_a^T H_a + H_b^T H_b\hat{H}H_c^T H_c \end{bmatrix})$$

$$= rank(\begin{bmatrix} H_a^T H_a & H_b^T H_b \end{bmatrix} \begin{bmatrix} I \\ \hat{H}H_c^T H_c \end{bmatrix})$$

If $rank(H_c) = n$, then full rank is achieved. Otherwise, which means neither H_a nor H_c is with full rank n, then $rank(H_a^T H_a + H_b^T H_b\hat{H}H_c^T H_c) = n$ has to be satisfied which finalizes the proof

for strategy II.

Theorems 4.5 and *4.6* provide mathematical solutions to find the sub-matrices H_1 and H_2 such that eq. (5) and (6) hold. Together with *Proposition 3.1* and *3.2*, they also manifest that reconfiguring information structure and corresponding residual test are capable of securing the power system against malicious data attacks.
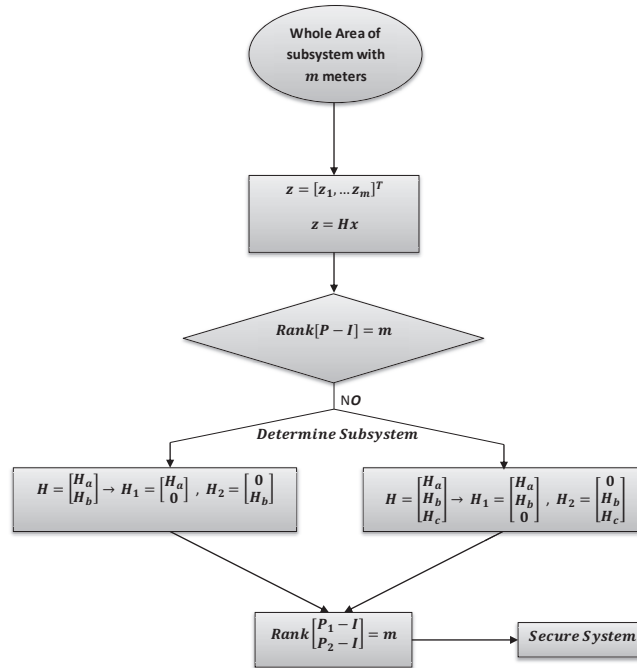
Figure 5.4: Protection scheme for Power system against malicious data attack

Remark 4.6: It is worth noting that $rank(\begin{bmatrix} A \\ C \end{bmatrix}) = m - n$ if and only if $H_a = 0_{l \times n}$. It implies that any row elimination of H will contribute the increase of rank. Until eliminating H_a with rank n, the full rank will be met. Also note that the full-rank requirement of H_1 and H_2 leads to $n \le l \le m - n$, which also indicates sufficient measures are required in the sense that $m \ge 2n$.

In what follows, an innovative protection scheme based on *Propositions 3.1, 3.2* and *Theorems 4.5, 4.6* are proposed in figure 5.4 for power system to enhance the security against malicious data attacks. It is a purely mathematical approach and does not require any physical effort either microgrid or network level in comparison with existing work.
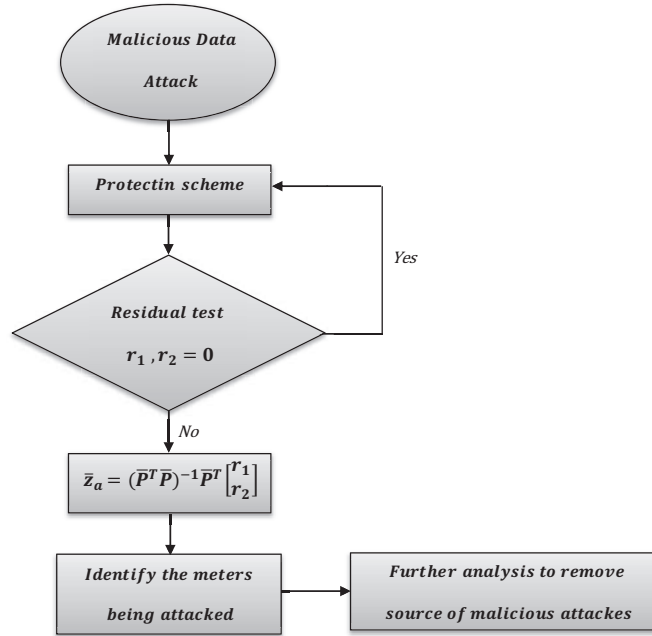
Figure 5.5: Identification scheme for Power system against malicious data attack

Bad meters identification formulation is shown in following section.

Identification

Vice verse, the identification scheme is also right on hand based on *Proposition 3.1* and *Theorem 4.5*. The meters that are being attacked by malicious data attack can be identified through the calculation of attack vector $\bar{z}_a$ given the residual vectors r_1 and r_2 generated by two sub-areas H_1

and H_2,

$$\bar{z}_a = (\bar{P}^T \bar{P})^{-1} \bar{P}^T \begin{bmatrix} r_1 \\ r_2 \end{bmatrix},$$ (5.19)

where $\bar{P} = \begin{bmatrix} P_1 - I \\ P_2 - I \end{bmatrix}$. It is true that all the meters corresponding to the non-zero elements in attack vector are being attacked. Further analysis can be performed to remove the sources of malicious data attack. The procedure of identification can be found in figure 5.5.

The performance of the proposed protection and identification schemes will be illustrated in the next section.

Illustrative Example and Results

In this section, a IEEE modified 30-bus system depicted in figure 5.6 is adopted to validate the effectiveness of proposed schemes. In terms of the system's setup , bus 1 is the reference bus ($\theta_1 = 0, V_1 = 1$) and the phase angles θ_2 up to θ_{30} are the state variables due to the simplicity. The voltage magnitude of each bus is assumed to be known. It is also assumed that the measurement vector z of system is given by a total set of 86 meters which measure 82 active/reactive branch flow and 4 power injection measurements. For more details, line data and operational point of the system are given in appendix A. The observation matrix $H \in \mathbb{R}^{86 \times 29}$ are all derived by partial derivative of available measurements with respect to state vector $\theta = \begin{bmatrix} \theta_2 & \cdots & \theta_{30} \end{bmatrix}^T$ as follows.
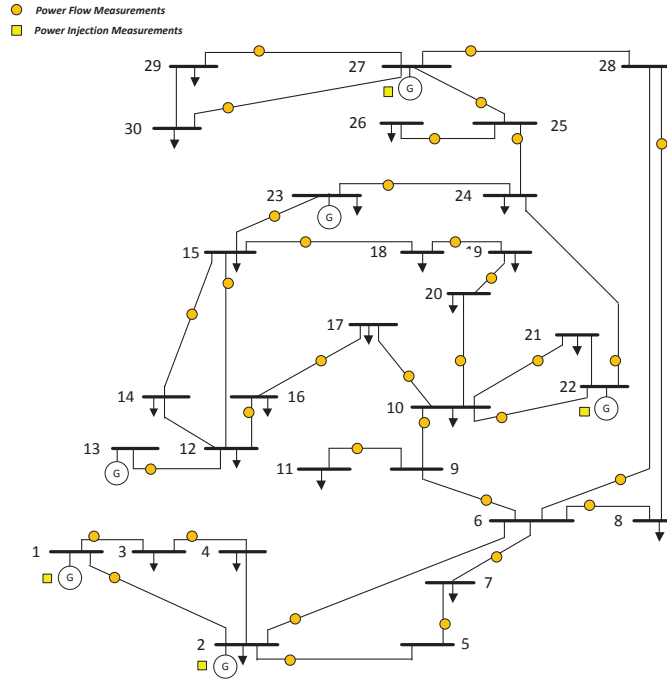
Figure 5.6: A single line diagram of modified IEEE 30-bus power system

Partial data has been omitted due to the limited space:

$$H = \begin{bmatrix} -15.0358 & 0 & \cdots & 0 & 0 & 0 \\ 0 & -4.8717 & \cdots & 0 & 0 & 0 \\ 5.1686 & 0 & \cdots & 0 & 0 & 0 \\ 0 & 22.6778 & \cdots & 0 & 0 & 0 \\ 4.6507 & 0 & \cdots & 0 & 0 & 0 \\ 4.9159 & 0 & \cdots & 0 & 0 & 0 \\ \vdots & \vdots & \cdots & \vdots & \vdots & \vdots \\ 0 & 0 & \cdots & 0 & 0 & 0.6279 \\ 0 & 0 & \cdots & 0 & -0.8509 & 0.8509 \\ 0 & 0 & \cdots & 1.3204 & 0 & 0 \\ 0 & 0 & \cdots & 4.7335 & 0 & 0 \\ 0 & 0 & \cdots & 0 & 0 & 0 \\ 0 & 0 & \cdots & 0 & 0 & 0 \end{bmatrix}$$

Note that $m = 86 > 58 = 2n$ guarantees the sufficient redundancy of measurements which is required in *Theorem 4.5*. It can be obtained that $rank(P - I) = 57 < 86$ and hence there are 29 linearly independent choices of coordinated attack vectors. In other words, 29 attack vectors are available to be used for injecting malicious data to corrupt the state estimation. By inspecting the

null space of $P - I$, the data attack vectors z_a which correspond to 86 meters are given in table I: (partial data has been omitted due to the limited space)

Table 5.1: Choices of Malicious Data Attack Vectors

z_a^1	z_a^2	z_a^3	$\cdots$	z_a^{27}	z_a^{28}	z_a^{29}
-0.0013	0.0010	-0.0003	$\cdots$	-0.0004	-0.0003	-0.0003
0.0006	-0.0003	0.0002	$\cdots$	0.0000	0.0001	0.0001
0.0066	0.0231	-0.0171	$\cdots$	-0.0514	0.0834	0.0488
0.0398	0.0126	-0.0120	$\cdots$	-0.0245	-0.0911	0.0055
0.0512	-0.0016	0.0137	$\cdots$	0.1520	-0.0147	0.0121
0.0199	-0.0303	0.0204	$\cdots$	0.0703	-0.2172	-0.0807
0.0524	0.0037	-0.0236	$\cdots$	-0.1269	-0.0262	-0.0841
$\vdots$	$\vdots$	$\vdots$	$\cdots$	$\vdots$	$\vdots$	$\vdots$
-0.3732	0.1800	-0.0984	$\cdots$	-0.0146	-0.0657	-0.0755
0.0027	-0.0580	0.0807	$\cdots$	0.0751	-0.0631	-0.0266
-0.0148	-0.0519	0.0385	$\cdots$	0.1156	-0.1874	-0.1097
-0.0766	-0.0242	0.0230	$\cdots$	0.0472	0.1752	-0.0105
-0.1201	0.0039	-0.0322	$\cdots$	-0.3565	0.0345	-0.0284
-0.0181	0.0276	-0.0185	$\cdots$	-0.0639	0.1976	0.0735

The adversary can choose any linear combination of these 29 non-zero attack vectors to inject malicious data and obviously $(P - I)z_a = 0$ holds. For more clarification, assume that the adversary is injecting z_a^1 to real measurement z. As we discussed earlier, this type of coordinated attack will

not be detected by the residual test since

$$E_1 = \|z + z_a^1 - H\bar{x}\| = 3.1187 \times 10^{-14}$$

which is almost zero and will be surely smaller than the pre-defined threshold C_T.

Next, the proposed schemes will be implemented for the illustration of effectiveness. What is more, the statistical analysis will be adopted to verify the equivalence between standard WLS state estimation and batch state estimation induced by our scheme.

Protection

By noticing the fact that there always exits malicious data attack vectors for the current system, we then follow the protection scheme depicted in Fig. 2 to secure the system. Via row operation, two sub-matrices H_1 and H_2 can be found by excluding 29 essential meters (independent rows) from the observation matrix H and setting zero for rest of the rows in each of them: (partial data has been omitted due to the limited space)

$$H_1 = \begin{bmatrix} 0 & 0 & 0 & \cdots & 0 & 0 & 0 \\ 0 & 0 & -0.0062 & \cdots & 0 & 0 & 0 \\ 0 & 0 & 0 & \cdots & 0 & 0 & 0 \\ 0 & 0 & 0 & \cdots & 0 & 0 & 0 \\ 0 & 0 & 0 & \cdots & 0 & 0 & 0 \\ 0 & 0 & 0 & \cdots & 0 & 0 & 0 \\ \vdots & \vdots & \vdots & \cdots & \vdots & \vdots & \vdots \\ 0 & 0 & 0 & \cdots & 0 & 0 & 0 \\ 0 & 0 & 0 & \cdots & 0 & 0 & 0 \\ 0 & 0 & 0 & \cdots & 0 & 0 & 0 \\ 0 & 0 & 0 & \cdots & -2.4294 & -1.8435 & -1.2754 \\ 0 & 0 & 0 & \cdots & 0 & -1.8435 & 0 \\ 0 & 0 & 0 & \cdots & 0 & 1.6560 & -1.6560 \end{bmatrix}$$

with $rank(H_1) = 29$, and another sub-matrix H_2 turns out to be: (partial data has been omitted due to the limited space)

$$H_2 = \begin{bmatrix} -15.0458 & -4.8725 & 0 & \cdots & 0 & 0 & 0 \\ 29.6883 & 0 & -5.1688 & \cdots & 0 & 0 & 0 \\ 4.8605 & 0 & 0 & \cdots & 0 & 0 & 0 \\ 0 & 1.1284 & 0 & \cdots & 0 & 0 & 0 \\ -1.6750 & 0 & 1.6750 & \cdots & 0 & 0 & 0 \\ 0 & 0 & 0 & \cdots & 0 & 0 & 0 \\ \vdots & \vdots & \vdots & \cdots & \vdots & \vdots & \vdots \\ 0 & 0 & 0 & \cdots & 0 & 0 & 0 \\ 0 & 0 & 0 & \cdots & 0 & 0 & 0 \\ 0 & 0 & 0 & \cdots & 0 & 0 & 0 \\ 0 & 0 & 0 & \cdots & -0 & 0 & 0 \\ 0 & 0 & 0 & \cdots & 0 & -0.8509 & 0.8509 \\ 0 & 0 & 0 & \cdots & 0 & 0.9256 & 0 \end{bmatrix}.$$

with $rank(H_2) = 29$. It can be shown that

$$rank \begin{bmatrix} P_1 - I \\ P_2 - I \end{bmatrix} = 86,$$

which validates the *Theorem 4.5*. Together with *Proposition 3.1*, it reveals that this reconfiguration of power system and corresponding residual test are able to secure the modified IEEE 30-bus system from any malicious data attack.

For more clarification, the following residual test is performed when the same attack vector z_a^1 is applied:

$$E_2^1 = \|z + z_a^1 - H_1 \bar{x}_1\| = 1.2063,$$

or

$$E_2^2 = \|z + z_a^1 - H_2 \bar{x}_2\| = 1.0893,$$

which is obviously easier to be detected with the pre-defined threshold C_T comparing to residual test E_1. It can be observed that the malicious attack vectors are no longer 'stealth' within the proposed protection scheme such that the effectiveness of proposed protection scheme is validated.

Identification

In this subsection, the effectiveness of identification scheme will be examined. Given the residual vectors r_1 and r_2 caused by z_a^1 regarding sub-areas H_1 and H_2,

$$r_1 = \begin{bmatrix} 0.0000 & 0.0000 & \cdots & -0.1201 & -0.0181 \end{bmatrix}^T,$$

and

$$r_2 = \begin{bmatrix} -0.0013 & 0.0006 & \cdots & -0.1211 & -0.0286 \end{bmatrix}^T.$$

Via eq. (15), we can calculate the attack vector $\bar{z}_a^1$ as follows,

$$\bar{z}_a^1 = \begin{bmatrix} -0.0013 & 0.0006 & \cdots & -0.1201 & -0.0181 \end{bmatrix}^T \approx z_a^1$$

Then, we can conclude that all the meters are being attack except meters 2, 25, 40, and 79 since the elements in the attack vector associated with these meters are zero. Furthermore, analysis can be performed to remove the sources of malicious data attack.

Statistical Analysis

For the estimation's purpose, the estimation algorithm under the proposed strategies turns out to be a two-batch estimation algorithm since we partition the whole system by two. Essentially, it is important to see the batch estimation is as good as the standard WLS estimation algorithm from the statistical perspective. Thus, the following covariance analysis from [85] is needed:

$$Cov(\hat{x}, \hat{x}) = \sigma^2 (H^T H)^{-1}$$

where the σ^2 is a variance of measurement error.

Assume that the $\hat{x}_1$ is the estimation of the state variables using H_1 and $\hat{x}_2$ is the estimation of the state variables using H_2. It is natural to realize that the estimation of two-batch algorithm $\bar{\hat{x}}$ is the average of these two state estimations. Then, the covariance of two-batch estimation algorithm is calculated as below

$$Cov(\bar{\hat{x}}, \bar{\hat{x}}) = Cov(\frac{\hat{x}_1 + \hat{x}_2}{2}, \frac{\hat{x}_1 + \hat{x}_2}{2})$$
$$= \frac{1}{4}\sigma^2(H_1^T H_1)^{-1} + \frac{1}{4}\sigma^2(H_2^T H_2)^{-1}.$$

For illustrating the equivalence of two algorithms, the well-known Frobenius norm [86] is needed to test the equality of these two covariance matrices

$$d^2 = \frac{1}{n}trace(Cov(\hat{x}, \hat{x}) - Cov(\bar{\hat{x}}, \bar{\hat{x}}))^2$$

where d is the distance between two covariance matrices, n is the number of states. It is clear that if two covariance matrices is exactly the same, i.e., $Cov(\hat{x}, \hat{x}) = Cov(\bar{\hat{x}}, \bar{\hat{x}})$, then $d = 0$. Through the calculation,

$$d^2 = \frac{1}{29}trace(Cov(\bar{\hat{x}}, \bar{\hat{x}}) - Cov(\hat{x}, \hat{x}))^2 = 0.2425$$

$$\implies d = 0.4925$$

which indicates the approximate equivalence between two algorithms. It is shown that the proposed scheme makes the power system secure from any malicious cyber-physical data attack with the reconfigured information structure and corresponding residual test, which does not require any physical effort comparing to the solutions in the literature. Furthermore, the identification scheme is capable of identifying the meters being attacked and further analysis can be performed to remove the sources of these attacks.

CHAPTER 6: CONCLUSIONS

The contribution of this dissertation comes in three major categories. The major power objective proposed in the first category of our research is the microgrid voltage and frequency stabilization after disconnecting from the main grid. Based on this objective, chapter 2 briefly introduces the inverter dynamic model and distributed cooperative secondary voltage and frequency control. Then the problem of single and multi-pinning of distributed cooperative secondary control of DGs in the microgrid islanding operation was formulated. In this chapter, it has been shown that the intelligent selection of a pinning set based on the number of its connections and distance of leader DG(s) from the rest of the network strengthened the microgrid's voltage and frequency regulation performance both in transient and steady state. In chapter 3, the proposed control strategy and algorithm was validated by simulation in MATLAB/SIMULINK using different microgrid topologies. Results indicated that it was easier to stabilize the microgrid's voltage and frequency in islanding mode operation by specifically placing the pinning node(s) on the DGs with high degrees of connectivity than by randomly placing pinning node(s) into the network. It has been shown the placement of the pinning node(s) was affected by the topology of the microgrid and its communication network. In all of these research study cases, DGs were required to only communicate with their neighboring units which facilitated the distributed control strategy.

Next, in chapter 4, the secondary adaptive voltage and frequency control of distributed generators in low and medium voltage microgrid in autonomous mode was proposed to overcome the drawback of existing traditional droop based control methods. For distributed power generation, the assumption of a purely inductive network does not hold. Our proposed secondary control strategy is adaptive with line parameters and can be applied to all types of microgrids, i.e., resistive, inductive, and unbalanced line parameters, to address the simultaneous impacts of active and reactive power fluctuations on the microgrids voltage and frequency. Simulation results validated the ef-

fectiveness of the proposed controller in the microgrid with different line parameters. In addition, in this chapter, an adaptive secondary voltage and frequency gain controller was proposed. The proposed adaptive controller takes into account the uncertainty in the microgrid and communication network parameters. The proposed adaptive control scheme, applied together with DG droop controls and secondary cooperative voltage and frequency controller to real time, calculated the voltage and frequency gain controller and weights of communication links in microgrid to minimize system transients in the islanding process and to ensure the microgrid's voltage and frequency stability. In the proposed method, each DG requires its own information and the information of its neighboring DG(s) on the communication network.

Finally, the security of power systems against malicious cyberphysical data attacks was studied in chapter 5. An algebraic condition for trustworthy power system to evade malicious data injection was proposed. The proposed method does not require any physical effort in either microgrid or network level. A well-known IEEE 30-bus system was adopted to demonstrate the effectiveness of the proposed schemes.

APPENDIX : SIMULATION PARAMETERS

Networks and Inverters Parameters

The specifications of the DGs, lines, and loads for four bus and five bus system are as follows:

Network Parameters of 4 Bus System

Line and Load Parameters			
Parameters	Values	Parameters	Values
Line12	0.23+j0.099	Load1	12KW+j12KVar
Line23	0.35+j0.580		
Line34	0.23+j0.099	Load2	15.3KW+j7.6KVar

DG's Parameters of 4 Bus System

Inverter Parameters			
DG1 and DG2		DG3 and DG4	
Parameters	Values	Parameters	Values
m_p	9.4×10^{-5}	m_p	12.5×10^{-5}
n_Q	1.3×10^{-3}	n_Q	1.5×10^{-3}
R_c	$0.03\ \Omega$	R_c	$0.03\ \Omega$
L_c	$0.35\ mH$	L_c	$0.35\ mH$
R_c	$0.1\ \Omega$	R_c	$0.1\ \Omega$
L_f	$1.35\ mH$	L_f	$1.35\ mH$
C_f	$50\ \mu F$	C_f	$50\ \mu F$
K_{PV}	1	K_{PV}	1
K_{IV}	4	K_{IV}	4
K_{PC}	5	K_{PC}	5
K_{IC}	8	K_{IC}	8

Network Parameters of 5 Bus Ring System

Load and Line Parameters			
Parameters	Values	Parameters	Values
Line12	$0.23+j0.01$	Load1	12KW+j12KVar
Line23	$0.23+j0.01$		
Line34	$0.23+j0.01$	Load2	15.3KW+j7.6KVar
Line45	$0.23+j0.01$		
Line51	$0.23+j0.01$		

Network Parameters of modified IEEE 6 Bus system

Load and Line Parameters			
Parameters	Values	Parameters	Values
Line12	$0.8+j0.8$	Load1	12KW+j12KVar
Line16	$0.8+j0.8$		
Line23	$0.8+j0.8$		
Line25	$0.8+j0.8$	Load2	12KW+j7.6KVar
Line34	$0.23+j0.8$		
Line45	$0.23+j0.1$	Load3	12KW+j7.6KVar
Line56	$0.23+j0.1$		

Network Parameters of Alternative 5 Bus System

Load and Line Parameters			
Parameters	Values	Parameters	Values
Line12	0.23+j0.01	Load1	12KW+j12KVar
Line23	0.23+j0.01		
Line34	0.23+j0.01		
Line45	0.23+j0.01		
Line51	0.23+j0.01	Load2	12 KW+j12KVar

DG's Parameters of 5 Bus System

Inverter Parameters			
DG1, DG2 and DG5		DG3 and DG4	
Parameters	Values	Parameters	Values
m_p	9.4×10^{-5}	m_p	12.5×10^{-5}
n_Q	1.3×10^{-3}	n_Q	1.5×10^{-3}
R_c	0.03Ω	R_c	0.03Ω
L_c	$0.35 \, mH$	L_c	$0.35 \, mH$
R_c	$0.1 \, \Omega$	R_c	0.1Ω
L_f	$1.35 \, mH$	L_f	$1.35 \, mH$
C_f	$50 \, \mu F$	C_f	$50 \, \mu F$
K_{PV}	1	K_{PV}	1
K_{IV}	4	K_{IV}	4
K_{PC}	5	K_{PC}	5
K_{IC}	8	K_{IC}	8

LIST OF REFERENCES

[1] "International energy outlook 2013," U.S. energy Information administration, Chapter 5: Electricity, Fig. 83. World net electricity generation by fuel, 2010-40 [Online]. Available: http://www.eia.gov/forecasts/archive/ieo13/pdf/0484(2013).pdf.

[2] An Interdisciplinary MIT study (Dec 2011), "The Future of electric Grid," [Online] Available: http://mitei.mit.edu/publications/reports-studies/future-electric-grid.

[3] R. Lasseter, "MicroGrids," in Proc. 2002 IEEE Power Eng. Soc.Winter Meeting (Cat. No.02CH37309), 2002, vol. 1, pp. 305-308.

[4] R. H. Lasseter, "Microgrids and distributed generation," J. Energy Eng., vol. 133, no. 144, 2007.

[5] M. Shahidehpour, "Role of smart microgrid in a perfect power system," in Proc. IEEE Power Energy Soc. Gen. Meeting, Minneapolis, MN, USA, 2010.

[6] "DOE Microgrid Workshop Report,"Microgrid Exchange Group, pp. 1?26, Aug. 2011. [Online]. Available: http://energy.gov/oe/downloads/ microgrid-workshop-report-august-2011

[7] A. Khodaei, "Provisional microgrid," IEEE Transactions on Smart Grid, VOL. 6, NO. 3, MAY 2015.

[8] A. Mehrizi-Sani and R. Iravani, "Potential-function based control of a microgrid in islanded and grid-connected models," IEEE Trans. Power Syst., vol. 25, pp. 1883-1891, Nov. 2010.

[9] Y. A. R. I. Mohamed and A. A. Radwan, "Hierarchical control system for robust microgrid operation and seamless mode transfer in active distribution systems," IEEE Trans. Smart Grid, vol. 2, pp. 352-362, Jun. 2011.

[10] Bidram, A., Davoudi, A.: "Hierarchical structure of microgrids control system," IEEE Trans. Smart Grid, 2012, 3, (4), pp. 1963-1976.

[11] K. D. Brabandere, B. Bolsens, J. V. den Keybus, A. Woyte, J. Driesen, and R. Belmans, "A voltage and frequency droop control method for parallel inverters," IEEE Transactions on Power Electronics, vol. 22, pp. 1107-1115, 2007.

[12] M. Chandorkar and D. Divan, "Decentralized operation of distributed ups systems," in Proc. IEEE PEDES, 1996, pp. 565-571.

[13] M. Prodanovic and T. Green, "High-quality power generation through distributed control of a power park microgrid," IEEE Transactions on Power Delivery, vol. 53, pp. 1471-1482, 2006.

[14] M. N. Marwali, J.-W. Jung, and A. Keyhani, "Control of distributed generation systems part ii: load sharing control," IEEE Transactions on Power Electronics, vol. 19, pp. 1551-1561, 2004.

[15] S. Parhizi, H. Lotfi, A. Khodaei, and S. Bahramirad, "State of the Art in Research on Microgrids: A Review," IEEE Journals and Magazines, vol. 3, pp. 890-925, July 2015.

[16] A.Mehrizi-Sani, A. H. Etemadi, D. E. Olivares, and R. Iravani, "Trends in microgrid control," IEEE Trans. Smart Grid, to be published.

[17] Guerrero, J.M., Vsquez, J.C., Matas, J., Castilla, M., Vicua, L.G.d., Castilla, M.: "Hierarchical control of droop-controlled AC and DC microgrids : A general approach toward standardization," IEEE Trans. Ind. Electron., 2011, 58, (1), pp. 158-172.

[18] Ilic, M.D., Liu, S.X.: "Hierarchical power systems control: its value in a changing industry," (Springer, London, UK, 1996).

[19] Ren, W., Beard, R.W., "Distributed Consensus in Multi-vehicle Cooperative Control: Theory and Applications," Springer, London (2009).

[20] R. Olfati-Saber, J. Fax, and R. M. Murray, "Consensus and cooperation in networked multi-agent systems," Proceedings of the IEEE, vol. 95, pp. 215-233, Jan. 2007.

[21] Xin, H., Qu, Z., Seuss, J., Maknouninejad, "A self-organizing strategy for power flow control of photovoltaic generators in a distribution network," IEEE Trans. Power Syst. 26, pp. 1462-1473, 2011.

[22] J. W. Simpson-Porco, F. Drfler, and F. Bullo, "Synchronization and power sharing for droop-controlled inverters in islanded microgrids," Automatica, vol. 49, no. 9, pp. 2603-2611, Sep. 2013.

[23] L. Y. Lu, and C. C. Chu, "Autonomous power management and load sharing in isolated micro-grids by consensus-based droop control of power converters," Future Energy Electronics Conference (IFEEC), 2013, pp.365-370, Nov. 2013.

[24] J. Y. Kim, J. H. Jeon, S. K. Kim, C. Cho, J. H. Park, H. M. Kim, and K. Y. Nam, "Cooperative control strategy of energy storage system and microsources for stabilizing the microgrid during islanded operation," IEEE Transactions on Power Electronics, vol. 25, no. 12, pp. 3037-3048, Dec. 2010.

[25] X. Li, X. Wang, and G. Chen, "Pinning a complex dynamical network to its equilibrium," Circuits and Systems I: Regular Papers, IEEE Transactions on, vol. 51, no. 10, pp. 2074 - 2087, Oct. 2004.

[26] H. Su, Z. Rong, M. Z. Q. Chen, X. Wang, G. Chen, and H. Wang, "Decentralized adaptive pinning control for cluster synchronization of complex dynamical networks," IEEE Trans. Cybernet., vol. 43, no. 1, pp. 394-399, Feb. 2013.

[27] X. Li, X. F. Wang, and G. R. Chen, "Pinning a complex dynamical network to its equilibrium," IEEE Trans. Circuits Syst. I, Reg. Papers, vol. 5, no. 10, pp. 2074-2087, Oct. 2004.

[28] W. Liu, W. Giu, W. Sheng, X. Meng, Sh. Xue, and M. Chen, "Pinning-Based Distributed Cooperative Control for Autonomous Microgrids Under Uncertain Communication Topologies,"IEEE Trans. Power Syst., vol. 31, no. 2, pp. 1320-1329, Mar. 2016.

[29] A. Bidram, A. Davoudi, F. L. Lewis, and J. M. Guerrero, "Distributed cooperative secondary control of microgrids using feedback linearization," IEEE Trans. Power Syst., vol. 28, no. 3, pp.3462-3470.

[30] S. Manaffam, and A. Seyedi, "Pinning control for complex networks of linearly coupled oscillators," in American Control Conference (ACC), 2013 , vol., no., pp. 6364-6369, June 2013.

[31] P. Delellis, M. Di Bernardo, and F. Garofalo, "Adaptive pinning control of networks of circuits and systems in Lur'e form," IEEE Trans. Circuits Syst. I, Reg. Papers, vol. 60, pp. 1-10, 2013.

[32] T. Chen, X. Liu, and W. Lu, "Pinning complex networks by a single controller," IEEE Trans. Circuits Syst. I, vol. 54, no. 6, pp. 1317-1326, Jun. 2007.

[33] F. Guo,C. Wen,J. Mao,J. Chen, and Y. Song, "Distributed Cooperative Secondary Control for Voltage Unbalance Compensation in an Islanded Microgrid," IEEE Transactions on industrial informatics, vol. 11, no. 5, October 2015.

[34] N. Pogaku, M. Prodanovic, and T. C. Green, "Modeling, analysis and testing of autonomous operation of an inverter-based microgrid," IEEE Trans. Power Electron., vol. 22, no. 2, pp. 613-625, Mar. 2007.

[35] A. Keyhani, M. N. Marwali, and M. Dai, "Integration of Green and Renewable Energy in Electric Power Systems," Hoboken, NJ, USA:Wiley, 2010.

[36] A. Bidram, A. Davoudi, F. L. Lewis, and Z. Qu, "Secondary control of microgrids based on distributed cooperative control of multi-agent systems," IET Gener. Transm. Distrib., vol. 7, no. 8, pp. 822-831, Aug. 2013.

[37] S. Manaffam, M. Talebi, A. Jain, and A Behal, "Synchronization in Networks of Identical Systems via Pinning: Application to Distributed Secondary Control of Microgrids," *IEEE Transactions on Control Systems Technology*, under review, available at https://arxiv.org/abs/1603.08844.

[38] H. A. Palizban, H. Farhangi, "Low Voltage Distribution Substation Integration in Smart Microgrid, " presented at ICPE 2011ECCE Asia, May 2011.

[39] A. Mehrizi-Sani and R. Iravani, "Potential-function based control of a microgrid in islanded and grid-connected models," *IEEE Transaction on Power System*, vol. 25, no. 4, pp. 18831891, Nov. 2010.

[40] V. Kounev, D. Tipper, A. A. Yavuz, B. M. Grainger, G. Reed"A Secure Communication Architecture for Distributed Microgrid Control," *IEEE Transactions on Smart Grid,* vol. 6, no. 5, September 2015.

[41] S. Adhikari, and F. Li "Coordinated V-f and P-Q Control of Solar Photovoltaic Generators with MPPT and Battery Storage in Microgrids,"

[42] H. Laaksonen, P. Saari, and R. Komulainen, "Voltage and frequency control of inverter based weak LV network microgrid,," presented at the Int. Conf. Future Power Syst., Amsterdam, The Netherlands, Nov. 18, 2005.

[43] J. A. P. Lopes, C. L. Moreira, and A. G. Madureira, "Defining control strategies for Micro-Grids islanded operation,," IEEE Trans. Power Syst., vol. 21, pp. 916924, 2006.

[44] B. Awad, J.Wu, and N. Jenkins,"Control of distributed generation," Electrotechn. Info. (2008), vol. 125/12, pp. 409414.

[45] A.Mehrizi-Sani, A. H. Etemadi, D. E. Olivares, and R. Iravani, "Trends in microgrid control," IEEE Trans. Smart Grid, to be published.

[46] F. Gao,and Iravani,"A control strategy for a distributed generation unit in grid-connected and autonomous modes of operation,"IEEE Trans. Power Deliv., 2008, 23, (2), pp. 850859.

[47] E. A. A. Coelho,P. C. Cortizo, and P. F. D. Garcia "Small-signal stability for parallel-connected inverters in stand-alone AC supply systems," IEEE Trans. Ind. Appl., 2002, 38, (2), pp. 533542.

[48] J. M. Guerrero, J. C. Vasquez, J. Matas, L. Garca de Vicuna, and M. Castilla, "Hierarchical control of droop-controlled AC and DC microgrids : A general approach toward standardization" in Proc. 2011 IEEE 8th ICPE ECCE, pp. 272279.

[49] A. Bidram, A. Davoudi, F. L. Lewis, and Z. Qu, "Secondary control of microgrids based on distributed cooperative control of multi-agent systems," IET Gener. Transm. Distrib., vol. 7, no. 8, pp. 822-831, Aug. 2013.

[50] F. Guo, C. Wen,J. Mao,J. Chen, and Y. Song,"Distributed Cooperative Secondary Control for Voltage Unbalance Compensation in an Islanded Microgrid," IEEE Transactions on industrial informatics, vol. 11, no. 5, October 2015.

[51] J. Y. Kim, J. H. Jeon, S. K. Kim, C. Cho, J. H. Park, H. M. Kim, and K. Y. Nam,"Cooperative control strategy of energy storage system and microsources for stabilizing the microgrid during islanded operation," IEEE Transactions on Power Electronics, vol. 25, no. 12, pp. 3037-3048, Dec. 2010.

[52] A. Bidram, and A. Davoudi, "Hierarchical structure of microgrids control system," IEEE Trans. Smart Grid, 2012, 3, (4), pp. 1963-1976.

[53] J. C. Vasquez, J. M. Guerrero, E. Gregorio, P. Rodriguez, R. Teodorescu, and F. Blaabjerg, "Adaptive droop control applied to distributed generation inverters connected to the grid," in Proc. 2008 IEEE ISIE, pp. 24202425.

[54] M. B. Delghavi and A. Yazdani, "A unified control strategy for electronically interfaced distributed energy resources," IEEE Transactions on Power Delivery, vol. 27, pp. 803812, 2012.

[55] J. C. Vasquez, J. M. Guerrero, M. Savaghebi, and R. Teodorescu, "Modelling, analysis and design of stationary reference frame droop controlled parallel three-phase voltage source inverters," , in Proc. 2011 IEEE 8th ICPE ECCE, pp. 272279.

[56] C. K. Sao, and P. W. Lehn, "Control and power management of converter fed microgrids," IEEE Trans. Power Syst., 2008, 23, (3), pp. 10881098.

[57] R. Majumder, A. Ghosh,G. Ledwich, F. Zare,"Load sharing and power quality enhanced operation of a distributed microgrid," IET Renew. Power Gener., 2009, 3, (2), pp. 109119.

[58] A. Engler, "Applicability of droops in low voltage grids," DER J., 2005, 1, pp. 15.

[59] Y. W. Li; C.N. Kao, "An accurate power control strategy for powerelectronics-interfaced distributed generation units operating in a low-voltage multibus microgrid," IEEE Trans. Power Electron., 2009, 24, (12), pp. 29772988.

[60] H. Han, Y. Liu, Y. Sun, M. Su, and J. M. Guerrero, "An Improved Droop Control Strategy for Reactive Power Sharing in Islanded Microgrid," IEEE Transactions on Power Electronics, 2015, Volume: 30, Issue: 6, pp. 3133-3141.

[61] J. M. Guerrero,L. G. De vicuna,J. Matas, M. Castilla, and J. Miret, "Output impedance design of parallel-connected UPS inverters with wireless load-sharing contro," IEEE Trans. Ind. Electron., 2005, 52, (4), pp. 11261135.

[62] E. Rokrok, and M. E. H. Golshan, "Adaptive voltage droop scheme for voltage source converters in an islanded multibus microgrid," IET Generation, Transmission Distribution, Volume: 4, Issue: 5, pp. 562-578, 2010.

[63] R. Majumder, G. Ledwich, A. Ghosh, S. Chakrabarti, and F. Zare, "Droop control of converter-interfaced microsources in rural distributed generation," IEEE Trans. Power Del., vol. 25, no. 4, pp. 27682778, Oct. 2010.

[64] H. Bevrani, and Sh. Shokoohi, "An Intelligent Droop Control for Simultaneous Voltage and Frequency Regulation in Islanded Microgrids," IEEE Transaction on Smart Grid, vol. 4, NO. 3,2013.

[65] J. M. Guerrero, J. Matas, L. Garcia de Vicuna, M. Castilla, and J. Miret, "Decentralized control for parallel operation of distributed generation inverters using resistive output impedance," IEEE Trans. Ind. Electron., vol. 54, no. 2, pp. 9941004, Apr. 2007.

[66] J. M. Guerrero, L. G. Vicuna, J. Matas, M. Castilla, and J. Miret, "A wireless controller to enhance dynamic performance of parallel inverters in distributed generation systems," IEEE Trans. Power Electron., vol. 19, no. 5, pp. 12051213, Sep. 2004.

[67] C. N. Rowe, T. J. Summers, R. E. Betz, D. J. Cornforth, and T. G. Moore, "Arctan powerfrequency droop for improved microgrid stability," IEEE Trans. Power Electron., vol. 28, no. 8, pp. 37473759, Aug. 2013.

[68] K. Brabandere,B. Bolsens,J. V. Keybus, A, Woyte, J. Driesen, and R. Belmans, " A Voltage and Frequency Droop Control Method for Parallel Inverters,"IEEE transaction on power electronics, vol. 22, NO. 4, July 2007

[69] E. Handschin, F. Schweppe, J. Kohlas, and A. Fiechter, "Bad data analysis for power system state estimation," IEEE Transactions on Power Apparatus and Systems, vol. 94, no. 2, pp. 329-337, 1975.

[70] Y. Liu, P. Ning, and M. K. Reiter, "False data injection attacks against state estimation in electric power grids," in Proc. ACM Conf. Comput. Commun. Security, Chicago, IL, Nov. 2009.

[71] K. Clements, G. Krumpholz, and P. Davis, "Power system state estimation residual analysis: an algorithm using network topology," IEEE Transactions on Power Apparatus and Systems, no. 4, pp. 1779-1787, 1981.

[72] A. Monticelli, "Electric power system state estimation," Proceedings of the IEEE, vol. 88, no. 2, pp. 262282, 2000.

[73] L. Xie, Y. Mo, and B. Sinopoli, "False data injection attacks in electricity markets," in 2010 First IEEE International Conference on Smart Grid Communications (SmartGridComm)., pp. 226-231,IEEE 2010.

[74] T. T. Kim and H. V. Poor, "Strategic protection against data injection attacks on power grids," IEEE Transactions on Smart Grid, vol. 2, pp.326-333, 2011.

[75] R. Bobba, K. Rogers, Q. Wang, H. Khurana, K. Nahrstedt, and T. Overbye, "Detecting false data injection attacks on dc state estimation," in CPSWEEK 2010, the First Workshop on Secure Control Systems, 2010.

[76] O. Kosut, L. Jia, R. Thomas, and L. Tong, "Malicious data attacks on the smart grid," IEEE Transactions on Smart Grid, no. 4, pp. 645-658,2011.

[77] G. Dan and H. Sandberg, "Stealth attacks and protection schemes for state estimators in power systems," in First IEEE International Conference on Smart Grid Communications (Smart-GridComm), pp. 214-219, 2010.

[78] A. Giani, E. Bitar, M. McQueen, P. Khargonekar, K. Poolla, and M. Garcia, "Smart grid data integrity attacks: Characterizations and counter- measures," In Proceedings of the IEEE SmartGridComm, October 2011.

[79] H. Sandberg, A. Teixeira, and K. H. Johansson, "On security indices for state estimators in power networks," In Preprints of the FirstWorkshop on Secure Control Systems, CPSWEEK 2010, Stockholm, Sweden, April 2010.

[80] K. C. Sou, H. Sandberg, and K. H. Johansson, "Electric power net- work security analysis via minimum cut relaxation," In Proceedings of the 50th IEEE Conference on Decision and Control, December 2011.

[81] Y. Yuan, Z. Li, and K. Ren, "Modeling load redistribution attacks in power systems," IEEE Transactions on Smart Grid, vol. 2. no. 2, pp. 382-390, Jun. 2011.

[82] A. Gomez-Exposito, A. Abur, A. de la Villa Jaen, and C. Gomez-Quiles, "A multilevel state estimation paradigm for smart grids," Proceedings of the IEEE, vol. 99, pp. 952-976, 2011.

[83] Ben-Israel Adi and Greville Thomas N.E., "Generalized Inverses," 2nd Edition, Wiley-Interscience, Chpt. 2, Sec.4, 2003.

[84] G. Marsaglia and G. P. H. Styan, "Equalities and inequalities for ranks of matrices. Linear and Multi-linear Algebra," Taylor Francis Online, pp. 269-292, vol. 2, 1974.

[85] R. W. Farebrother, "Linear least squares computations," Marcel Dekker INC, pp. 160, 1988.

[86] Muni S. Srivastava and Hirokazu Yanagihara, "Testing the equality of several covariance matrices with fewer observations than the dimension," Elsevier, Journal of Multivariate Analysis 101,pp.1323, 2010.

[87] R.D. Zimmerman and C.E. Murillo-Sanchez. MATPOWER, "A MATLAB Power System Simulation Package," http://www.pserc.cornell.edu/matpower/manual.pdf, September 2007.